1.0

2.8 2.5
3.2
3.6 2.2

4.0 2.0

1.1

1.8

1.25 1.4 1.6

MICROCOPY RESOLUTION TEST CHART

AFGL-TR-80-0129

LEVEL

QUANTITATIVE SIMULATION OF A MAGNETOSPHERIC SUBSTORM
2. Comparision With Observations

M. Harel
R. A. Wolf
R. W. Spiro
P. H. Reiff
C. -K. Chen
W. J. Burke
F. J. Rich
M. Smiddy

William Marsh Rice University
6100 South Main Street
Houston, Texas 77005

Scientific Report No. 3

23 January 1980

AIR FORCE GEOPHYSICS LABORATORY
AIR FORCE SYSTEMS COMMAND
UNITED STATES AIR FORCE
HANSCOM AFB, MASSACHUSETTS 01731

SCIENTIFIC-3

REPORT DOCUMENTATION PAGE

READ INSTRUCTIONS
BEFORE COMPLETING FORM

1. REPORT NUMBER	2. GOVT ACCESSION NO.	3. RECIPIENT'S CATALOG NUMBER
AFGL-TR-80-0129	AD-A087700	

4. TITLE (and Subtitle)	5. TYPE OF REPORT & PERIOD COVERED
Quantitative Simulation of a Magnetospheric Substorm. 2. Comparison with Observations	Scientific Report No. 3
	6. PERFORMING ORG. REPORT NUMBER

7. AUTHOR(s)	8. CONTRACT OR GRANT NUMBER(s)
M. Harel R. A. Wolf R. W. Spiro P. H. Reiff, C.-K. Chen, W. J. Burke, F. J. Rich and M. Smiddy	F19628-77-C-0005

9. PERFORMING ORGANIZATION NAME AND ADDRESS	10. PROGRAM ELEMENT, PROJECT, TASK AREA & WORK UNIT NUMBERS
William Marsh Rice University 6100 South Main St. Houston, Texas 77005	61102F 231161AM

11. CONTROLLING OFFICE NAME AND ADDRESS	12. REPORT DATE
U.S. Air Force Geophysics Laboratory Hanscom AFB Massachusetts 01731 Contract Monitor: Capt. David Hardy (PHG)	23 January 1980
	13. NUMBER OF PAGES
	80

14. MONITORING AGENCY NAME & ADDRESS(if different from Controlling Office)	15. SECURITY CLASS. (of this report)
	Unclassified
	15a. DECLASSIFICATION DOWNGRADING SCHEDULE

16. DISTRIBUTION STATEMENT (of this Report)

Approved for public release; distribution unlimited

17. DISTRIBUTION STATEMENT (of the abstract entered in Block 20, if different from Report)

18. SUPPLEMENTARY NOTES

19. KEY WORDS (Continue on reverse side if necessary and identify by block number)

Magnetosphere   Electric Fields
Ionosphere
Substorm
Ring Current

20. ABSTRACT (Continue on reverse side if necessary and identify by block number)

Abstract

Several results of the computer simulation of the behavior of the inner magnetosphere during the substorm-type event of 19 September 1976 are discussed, in detail.

(Please see other side)

The model predicts a modest ring-current injection, in to about L=6, with total strength that is approximately equal to the strength estimated from the observed decrease in Dst. For the geosynchronous-orbit region on the dusk side, the model predicts a characteristic energy dispersion often observed by McIlwain and collaborators, energetic ions arrive frist after substorm onset, followed by less energetic ions.

The computed electric fields compare satisfactorily with electric fields measured from S3-2, although there are detailed differences. Three general features on which the model and observations are in good agreement are: (1) the magnitude and direction of the high-latitude electric field; (2) the degree to which the low-latitude ionosphere is shielded from the high-latitude convection electric field; (3) the fact that the poleward electric field on the dusk side is significantly larger, on the average, than the equatorward electric field on the dawn side. The observations indicated one instance of rapid flow equatorward of the auroral zone, involving an electric field of more than 100 mV/m. This rapid subauroral flow was accurately predicted by the model.

The predicted east-west magnetic perturbations due to region-2 Birkeland currents agree satisfactorily with S3-2 observations with regard to direction, total magnitude and general location, but there is an important general discrepancy: in most cases, the actual Birkeland currents were distributed over a wider range of latitude than the model would predict. Speculations are presented as to possible explanations of discrepancy.

The model Birkeland currents agree satisfactorily with the averaged observations of Iijima and Potemra, in terms of direction, strength and overall pattern. The model suggests a theoretical interpretation of the observed overlap region near midnight, where a region of upward Birkeland current is bounded on its equatorward and poleward sides by regions of downward current.

The model provides a useful picture of the overall magnetosphere-ionosphere current system. It also suggests that the observed asymmetry in the change of the horizontal magnetic field at low-latitude ground stations during the main phase of a magnetic storm should be interpreted primarily in terms of the sum of two effects: (a) a partial ring current centered near local midnight and associated region-2 Birkeland currents, and (b) net downward Birkeland current near local noon, upward at night.

The model indicates that the total Joule heating during the event is about 2-3 times the increase in ring-current energy, a result that is in apparent contradiction to some previous estimates. A general, but highly approximate, analytic argument is presented in support of this result of the simulation. Some simple formulas are presented that give rough estimates of global Joule-heating rates from observable parameters.

I. INTRODUCTION

In this and the succeeding paper [Spiro et al. (1980), hereinafter referred to as Paper 3], we discuss in detail several particularly interesting aspects of our "first try" simulations of the substorm-type event that occurred 19 September 1976. Whenever possible, we compare directly with data -- either data taken 19 September 1976 or average substorm data from other time periods.

This paper deals with observational comparisons and implications of the simulations, for L-values greater than about 6. Paper 3 will discuss similar issues for lower L-values. We hope later to produce an additional paper, which will deal with comparison with ground magnetograms.

Harel et al. (1980), in what is hereinafter referred to as Paper 1, describe the logic of the computer model, specify the inputs used and present an overview of results.

In Section II of the present paper, we discuss injection of the model ring current and the relationship of the model to certain classic observations of McIlwain and others. In Sections III and IV, we make direct comparisons between predicted Birkeland currents and ionospheric electric fields, and the corresponding S3-2 observations, from 19 September 1976. In Section V, we describe the overall three-dimensional current configuration implied by our model and compare it with earlier ideas and with TRIAD data. In Section VI, we address an important aspect of the energetics of the system, namely the comparison between the amount of energy dissipated in Joule heating of the ionosphere and the amount invested in the ring current.

II. INJECTION OF THE RING CURRENT

A. General Discussion

Our model simulates the gradual, asymmetric development of a ring current during a substorm-type event. Unfortunately, no direct confrontation with ring-current-particle data for 19 September 1976 is possible. The only satellite that was in the ring-current region on 19 September 1976 and could make plasma measurements was ATS-6. Unfortunately, ATS-6 was near local noon during the simulated event, and, as discussed in Paper 1 and below, we have numerical-analysis problems near local noon. Also, in these initial simulation runs, we did not keep track of the absolute electron inner edge, but only the boundaries representing 25% and 75% precipitation; because we assumed electron loss by strong-pitch-angle scattering, the model electron inner edge was strongly eroded, and the 25% and 75% loss boundaries remained outside of synchronous orbit. Thus from our initial simulation runs we can make no accurate predictions with regard to electrons at synchronous orbit. Although no direct confrontation is possible with data for 19 September 1976, we can compare model results with features of ion fluxes generally observed during substorms.

Figures 1 and 2 show the computed global distribution in the equatorial plane of the total electric field and the resulting $\underline{E} \times \underline{B}/B^2$ velocity flow field at 1050 UT, which approximately corresponds to the peak of the substorm expansion. The displayed total electric field is a superposition of the convection electric field (roughly dawn-dusk, but greatly distorted due to conductivity inhomogeneities and the effects of region-2 Birkeland currents), the electric field due to the earth's
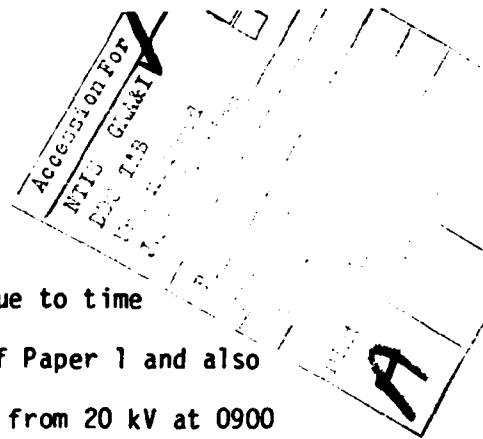
rotation, and the induction electric field, which is due to time variations in our magnetic-field model (see Figure 8 of Paper 1 and also below). The increase in the cross-tail potential drop from 20 kV at 0900 UT to 80 kV at 1040 UT, combined with the induction electric field, which is westward near local midnight between 1000 and 1040 UT (see Figure 3), causes the inner edge of the plasma-sheet ions to move in from ≈ 8-9 R_E geocentric distance on the nightside at 0900 UT to $\approx$ 6-7 R_E geocentric distance at 1040 UT.

Figure 4, which is based partly on information from Figures 23-26 of Paper 1, shows the time development of the inner edge of four different ion components of our computed plasma sheet, namely λ = 478, 1730, 3880 and 8650 eV $R_E^{2/3}\gamma^{-2/3}$, where the energy invariant λ was defined in equation 1 of Paper 1. The diagrams show the tendency of the more energetic ions to drift westward to form a complete ring. It is not clear that low-energy ions will form a complete ring.

Unfortunately, a numerical difficulty with our program prevented the ring from crossing local noon. For the energy component shown in Figure 4d, the most energetic and thus the fastest-drifting ions that we considered, the particles were, at 1150 UT and 1300 UT, being artificially held near local noon. Examination of the particle drift velocities indicates that the inner edge for λ = 8650 at 1300 UT will actually look like the boundary shown schematically by the curve with small circles on it in Figure 4d. The simulation was terminated at 1300 UT, when the program was holding several of our ion species near local noon.

B. Ion Arrival Times

It is interesting to consider the arrival times of ions of various energies at synchronous orbit near dusk. Before presenting numerical results for these arrival times, we should discuss some of the competing effects involved. In their recent review, Kivelson et al. (1979) have emphasized the importance of distinguishing between the effect of a geosynchronous satellite moving into a static plasma structure, and a dynamic event involving real time-dependence of the magnetosphere, since the two effects may be hard to differentiate in the data from a single satellite. In our discussion, we shall explicitly restrict ourselves to dynamic effects, by considering what would be observed by a "satellite" at a fixed location in solar-magnetospheric coordinates.

Within the category of dynamic events, we could further distinguish a special class, namely quasistatic events, in which the electric-field changes are so slow that the particle distribution at time t is near the equilibrium configuration corresponding to the electric-field configuration at time t. Much theoretical work has been done within this convenient approximation. (See review by Kivelson et al. (1979).) Within this approximation, the inner edge of the plasma sheet, from the point of view of particles of a certain λ, coincides with the Alfvén layer for that λ, namely the boundary between trajectories that go from the magnetospheric tail to the magnetopause and trajectories that circle the earth or some other region in the inner magnetosphere.

Figure 5 compares computed radial distances of inner edges and instantaneous Alfvén layers at about 1820 MLT, for various universal times. The complicated equivalent-potential diagrams of low-energy ions

(e.g. Figure 23 of Paper 1) have been discussed thoroughly in the literature (see Kivelson et al. (1979) and references therein) and will therefore not be discussed in detail here.

From Figure 5, we conclude the following:

(1) The system started out at 0900 rather far from "equilibrium". (For the purpose of the present discussion, we define "equilibrium" as coincidence of the Alfvén layers and corresponding plasma-sheet-component inner edges near local dusk.)

(2) From 0900 to 1000- ϵ, a period of rapidly increasing polar-boundary potential drop, the distance from "equilibrium" increases slightly. Between 1000- ϵ and 1000+ ϵ, the system moves sharply away from "equilibrium", due to the sudden conductivity enhancement and consequent reduction in shielding. From 1000+ ϵ to 1050, shielding gets better despite the increasing polar-cap potential drop, and the system begins a partial move toward "equilibrium". By 1050, the fastest-drifting, highest-energy component ($\lambda = 8650$) is close to "equilibrium". After 1050, with now a steady polar-boundary potential drop, the system moves toward a steady state, and, as time passes, lower energy particles approach "equilibrium". At 1300 UT, species with $\lambda \geq 1700$ eV $R_E^{2/3} \gamma^{-2/3}$ are close to "equilibrium", but less energetic particles are not. (For a global view of this approach to steady-state, see Figures 23-26 of Paper 1.)

(3) Both Alfvén layers and inner edges move. Consider the period 1050 to 1300 UT, when the polar-cap potential drop was held constant and the system gradually approached steady-state. For $\lambda = 1700$ eV $R_E^{2/3} \gamma^{-2/3}$, the approach to "equilibrium" is less a matter of inner edges moving earthward than of Alfvén layers moving outward, as the shielding becomes

more and more complete.

(4) The species with Alfvén layers that penetrate closest to the earth
are the low-energy ions (λ = 500 to 1100, corresponding to ~ 3 to 8 keV at
L = 6.6). However, after substorm onset, the particles whose inner edges
penetrate closest to the earth near dusk are the more energetic ions
(λ = 1730 to 8650, corresponding to energies of ~12 keV to 60 keV at
L = 6.6). This effect -- the energetic ions being the best penetrators
at dusk -- is purely dynamic, and is a temporary substorm phenomenon.
The message that there has been a rapid substorm-associated inward motion
near midnight propagates westward fastest for the more energetic ions,
because of their greater drift speed.

Figure 6 shows what an observer stationed near geosynchronous
orbit (L = 6.6) near dusk would see as a function of universal time, as
predicted by our various computer runs. High-energy (35-50 keV) ions
would be detected first at about 1100 UT (an hour after onset). As time
progressed, lower and lower energy ions would appear.

Similar behavior has been observed many times by McIlwain and
collaborators (see, e.g., DeForest and McIlwain, 1971) on geosynchronous
satellites and also by Konradi et al. (1976) on satellite S^3.
Encouragingly, this basic energy dispersion in arrival times is a natural
result of our self-consistent calculation. Roederer and Hones (1974)
obtained similar results using an assumed electric field distribution and
McIlwain (1974) has constructed detailed time-independent electric-field
models to fit observed arrival times for both ions and electrons, but in
neither case was the electric field computed self-consistently.

This characteristic duskside dispersion effect, with ~ 50 keV ions

arriving first, followed by ions of lower and lower energy, is a purely dynamic effect. In an injection event consisting of a quasistatic plasma-sheet structure moving in over the satellite, one would see ions of ~ 3 keV first, followed by ions of lower and higher energies. (See Figure 5.)

Although our model induction electric field is generally much smaller than the potential electric field in the inner magnetosphere, in one critical respect the induction field dominates, namely the westward electric field close to the inner edge of the plasma sheet near midnight (see Figures 1 and 3). It is mostly this westward electric field that injects the ring current. Thus one would be tempted to say that the induction field plays a dominant role in ring-current injection.

To test the effect of the induction electric field on ring-current injection, we did a computer experiment (labelled run 3 in the notation of Table 2, Paper 1), in which we redid run 2 with a time-independent magnetic field and thus no induction electric field. The result, in terms of ion arrival times, is shown in Figure 6c. Surprisingly, elimination of the induction electric field makes little difference in ring-current location or energy dispersion, the only significant difference being that our highest energy ions, ~ 60 keV, did not penetrate quite to L = 6.6. It turned out that elimination of the westward induction electric field near midnight decreased the eastward ring-current polarization field there, leaving the total westward electric field almost the same.

We cannot safely conclude, however, from this one computer experiment, that the induction electric field due to collapse of the tail

field has little effect on ring-current injection. Tests of other cases are needed, particularly cases in which the westward electrojet builds up over a shorter time span than in our case (40 minutes). However, the experiment does demonstrate the compensating tendencies of the polarization electric fields generated at the inner edge of the model ring current -- electric fields that oppose any deformation of the ring current.

We note that Figure 6, and particularly Figure 6c, bear a general resemblance to ion nose events, as observed early in magnetic storms, for example at $L \approx 5$ by Smith and Hoffman (1974); they observe large ion fluxes in an energy band of increasing width, with a maximum energy of a few tens of kilovolts.

It may be that, as suggested by Lyons and Williams (1979), a pre-existing ring current can play a significant role in the creation of a storm-time ring current. That is, a substorm, in addition to injecting plasma-sheet plasma, newly arrived from the magnetotail, may inject some already-trapped ions onto new trapped orbits closer to the earth. For simplicity, such pre-existing ring-current plasma was ignored in these first-try simulations; it will be included in the next runs of our simulation effort, to help evaluate the importance of the Lyons-Williams suggestion.

Nevertheless, these first efforts at detailed theoretical modeling of a ring-current injection, using self-consistently computed electric fields, have been very encouraging. Enhanced convection automatically led to injection of a reasonable ring current, and there is no obvious theoretical necessity for invoking more exotic processes for explaining

the bulk of the ring current, such as injection of ions from the midlatitude ionosphere and outer plasmasphere directly into the ring current, as proposed by C. E. McIlwain. Of course, direct ion injection into the ring current does occur to some extent, but we regard it as a perturbation effect. More simulations, with precise comparison with data, should help clarify the situation. For more discussion of this point, see Wolf and Harel (1979).

III. COMPARISON OF THEORETICAL ELECTRIC FIELDS AND
BIRKELAND CURRENTS WITH DIRECT OBSERVATIONS

A. Format and Assumptions Used for Figures 7-12

Figures 7-12 display detailed comparisons of theoretically computed electric fields and transverse-magnetic-field variations with the corresponding observed quantities, for the six passes of satellite S3-2 through the auroral zone during the simulated event of 19 September 1976. Also shown are computed Birkeland-current densities, averaged over latitude bins $\approx 0.4°$ wide. The data shown are replots, on a different scale, of data shown in Figures 4-6 of Paper 1.

One of the important features of our computer simulation, of course, is its ability to predict global patterns of electric fields and currents during the substorm. (See Figures 11-20 in Paper 1.) When specific satellite data become available we therefore can simply map the ionospheric electric field along magnetic field lines to the satellite track and compare the measurements with our theoretical predictions. This procedure is based on the assumption of no significant magnetic-field-aligned electric field. A similar comparison with S3-2 data is given in a previous paper (Harel et al., 1979). The present comparison and discussion, however, include the following improvements.

a) The theoretical electric-field curves are now not merely based on the computed potentials at our 21 x 28 grid points; they now utilize an algorithm for including the most important sub-grid-scale latitudinal structure, namely the structure due to Birkeland currents at the inner edges of the 41 plasma-sheet subspecies (corresponding to electrons and ions of various energies); this more accurate display scheme shows the

same latitudinal fine structure that we use to calculate motions of the various inner edges; equatorward of the inner-edge region, model electric fields are computed from grid-point potentials by simple symmetric differences;

b) Transverse magnetic fluctuations ΔB measured by the magnetometer onboard S3-2 are now presented and compared with the corresponding theoretical ΔB's, computed using the formulae

$$\Delta B_{west} (\Lambda) = \mu_o R_E \int_{\Lambda_o}^{\Lambda} j_{up}(\Lambda') d\Lambda' \qquad \text{(dawnside northern hemisphere)} \qquad (1a)$$

$$\Delta B_{east} (\Lambda) = \mu_o R_E \int_{\Lambda_o}^{\Lambda} j_{down} (\Lambda') d\Lambda' \qquad \text{(duskside northern hemisphere)} \qquad (1b)$$

$$\Delta B_{east} (\Lambda) = \mu_o R_E \int_{\Lambda_o}^{\Lambda} j_{up} (\Lambda') d\Lambda' \qquad \text{(dawnside southern hemisphere)} \qquad (1c)$$

$$\Delta B_{west} (\Lambda) = \mu_o R_E \int_{\Lambda_o}^{\Lambda} j_{down}(\Lambda') d\Lambda' \qquad \text{(duskside southern hemisphere)} \qquad (1d)$$

where Λ = invariant latitude and j_{up} (j_{down}) is the vertically upward (downward) component of Birkeland-current density; Λ_o = an invariant latitude that is equatorward of all computed Birkeland currents.

The measured ΔB's shown in Figures 4-6 of Paper 1 represent differences between observed magnetic fields and a model of the earth's field. The measured ΔB's are thus due not only to local Birkeland currents but also to model inaccuracy and other errors. To make zero-order correction for these experimental problems, we have subtracted a smooth baseline from the curves shown in Figures 4-6 of Paper 1, to arrive at the ΔB's shown here in Figures 7-12. The most equatorward

portions of the ΔB's shown in Figures 7-12 are highly uncertain due to the difficulty of determining the appropriate baseline.

We stress that the theoretical electric fields and Δ B's shown are indeed theoretical results and not empirical curves constructed to fit the data. The logic of and inputs to the model were described in detail in Paper 1 and will not be discussed again here. However, we should stress that the only ways in which the theoretical curves were constrained to fit the data were the following:

(a) The latitudinal coordinate used in Figures 7-12 is labelled "Degrees from polar cap", by which we mean "Degrees invariant latitude from the poleward boundary of our calculation". Plotting this way corrects for the 1°- 4° difference between the nominal invariant latitude of our model boundary and the observed equatorward edge of the region-1 currents. (See Paper 1.)

(b) Since the polar- boundary potential drop is input to the model (see Paper 1), the sum of the dawnside and duskside integrals of $E_{forward}$ over the auroral zone is constrained to be approximately correct for each of the three passes shown in Figures 7-12.

We have not presented available data from two S3-2 satellite passes that occurred 5-6 hours before substorm onset (0400 and 0450 UT), although data from them were used to estimate the "quiet time" initial polar-cap potential drop (Figure 3b of Paper 1). The observed electric fields on those passes were relatively small but very complicated, and attempts to compare theory and data for these passes have proved unilluminating. Also, the measured spin-axis component of electric field is not displayed here in detail, because instrumental uncertainties in

that component are generally comparable to the very small measured or predicted values.

Although the TRIAD satellite made three polar passes during the modeled time period we have found no meaningful confrontations between the model and TRIAD data for 19 September 1976. Data from the three TRIAD passes, which were kindly provided to us by T. A. Potemra, generally do not extend significantly equatorward of our polar boundary. Comparisons with averaged TRIAD data are given in Section V.

The model makes detailed predictions as to the strength and distribution of region-2 Birkeland currents, but it also can be used to make rough estimates of region-1 currents, if we assume that the current entering our poleward boundary goes directly out along magnetic-field lines just poleward of our boundary. Table 1 compares model ΔB values estimated in this simple way with ΔB's estimated from the S3-2 data displayed in Figures 4-6 of Paper 1.

Discussion and Interpretation

The sawtooth structures on the theoretical E or ΔB curves in Figures 7-12 are indicative of the numerical method. Each vertical rise represents the electric-field jump or Birkeland current associated with the inner edge of the plasma sheet for one of our 41 sub-species of particles.

We should make some comments on points of agreement and disagreement between theory and observation.

a) There is little agreement regarding small details. Obviously, our model cannot duplicate small-scale fluctuations in data, some of which may be noise. Even some substantial fluctuations (e.g., the region

between 64° and 67° in Figure 9).due mainly to current sheets $\leq$ 30 km
wide, cannot be reproduced. Our grid system and conductivity model are
too coarse to handle them.

b) A characteristic dawn-dusk asymmetry appears both in the data and
theory. Namely, both in the model and in the data, the average electric
field and potential drop are larger on the dusk side than on the dawn
side. This effect, which Kelley (1976) noticed in balloon electric-
field data, is characteristic of the distortions in the ionospheric
electric field that are necessary to maintain current conservation, given
the situation that Hall currents flow antisunward across Hall-conductivity
drops at dawn and dusk (Wolf, 1970).

c) The low-latitude ionosphere is shielded effectively from the high-
latitude electric field, both in the theory and the data. The greatest
leakage through the shielding occurred, both in the theory and
the data, in the case shown in Figure 8. In the model, this penetration
resulted from the rapid conductivity changes at substorm onset, changes
to which the plasma-sheet inner edge, which causes the shielding, has not
had time to react. (For a theoretical discussion of shielding, see
Vasyliunas (1972), Jaggi and Wolf (1973), or Southwood (1977)).

d) Although measured and predicted ΔB's agree in a very general sense,
there is an interesting and significant discrepancy. The data often show
large changes in ΔB, representing substantial region-2 Birkeland currents,
poleward of the model region-2 Birkeland currents; this discrepancy appears
to be independent of most of the know inaccuracies in the model (results
of inadequately known boundary conditions, inaccurate conductivities,
etc.) Within the assumption that plasma-sheet particles gradient, curvature

and $\underline{E} \times \underline{B}$ drift, they can connect to Birkeland currents only where there are gradients in the n_s's (see Equation 6 of Paper 1); further, if the particles drift in from the tail without loss, n_s is an invariant along a drift trajectory (see Appendix of Paper 1). However, the observed Birkeland currents imply that the n_s's increase systematically with geocentric distance, well beyond the normal inner-edge region. In the classic convection picture, with particles drifting adiabatically in from the tail, it is not clear how the n_s's could increase systematically with increasing radial distance, yet still be constant along drift trajectories. Thus the discrepancy between observed and predicted Region-2 Birkeland currents may be suggesting a flaw in the classic convection picture. Resolution of the discrepancy may require invoking an additional physical process, for example polarization drifts (see, e.g., Rostoker and Boström, 1976), substorm-associated loss of particles from certain plasma-sheet flux tubes (Erickson and Wolf, 1980), or conduction of current across magnetic-field lines at high altitudes, due to large-amplitude turbulence there. Also, it should be remarked that, in most cases, the data seem to imply weak Birkeland currents equatorward of the model Birkeland currents, although the data are admittedly inconclusive due to the baseline problems mentioned above. We suspect that these observed Birkeland currents, if real, connect to the ring current that remains from the geomagnetic storm of the previous day.

The case shown in Figure 12 is especially interesting and is discussed in detail in section IV.

IV. RAPID SUBAURORAL FLOW

The most striking feature of the data shown in Figures 7-12 is the sharp electric-field peak of more than 100 mV/m that is observed well below the polar-cap boundary in the last half of orbit 4079B-South (Figure 12). We refer to this feature as "rapid subauroral flow". Similar flows have been observed many times before -- often, but not always, in association with the midlatitude ionospheric trough (Spiro et al., 1974; Heelis et al., 1976; Smiddy et al., 1977; Maynard, 1978; Spiro et al., 1978).

One obviously exciting feature of Figure 12 is that, as shown in the top panel, all the computer runs (as described in Table 2 of Paper 1) predicted the observed rapid subauroral flow, and at roughly the right location. Note that the location of the peak of the rapid subauroral flow computed in run 4 differs from the observed location by only about a degree, approximately the precision to which we could observationally define the polar boundary. Also note that the other two runs show electric-field peaks that lie approximately a degree poleward of the run-4 peaks. This difference in model results is easy to understand physically: for run 4, we overestimated the polar-boundary potential drop; consequently the plasma-sheet ions were injected deeper into the magnetosphere than was the case for runs 1 and 2; thus the rapid subauroral flow, which should be bounded by the inner edge of the plasm-sheet/ring-current ions (Southwood and Wolf, 1978), extended to lower latitude for run 4 than for runs 1 or 2.

Our computer model shows rapid subauroral flows in the dusk-to-midnight sector, though not elsewhere, which is consistent with the previously mentioned observations. We should comment that no other

clear rapid subauroral flows were observed by S3-2 during this simulated
event; no other clear cases were predicted by the model for the S3-2
satellite path, although one computer run did predict a borderline case
of rapid subauroral flow for the duskside part of orbit 4079A-North
(Figure 9). The model generally predicts that, in the dusk-to-midnight
sector, the maximum poleward electric field occurs near the equatorward
edge of the convection region. (See Figures 8, 9 and 12.) However, the
peak in model electric field is dramatic enough to be called "rapid
subauroral flow" only when the ionospheric current connecting the
electron-precipitation zone with the inner edge of the ion plasma sheet
flows across a region of low conductivity, which requires large electric
fields. In our conductivity model, the auroral enhancement has a
smeared-out equatorward edge that is tied to the computed inner edge of
the ion plasma sheet. Low conductivity at the inner edge of the ion
plasma sheet thus occurs in the model only if the ion inner edge is
substantially equatorward of the electron inner edge, a situation that
occurs only on the dusk side and is encouraged by substantial
ring-current formation as the event progresses. In these respects, the
computer model behaves in accordance with the analytic model of Southwood
and Wolf (1978) and presumably in accordance with nature.

We should note one other interesting feature of the comparison in
Figure 12, panel 1, of the electric fields computed in three of the
computer runs. Namely, the run that produced the most pronounced peak
(though not the highest) is run 1, which had the sharpest conductivity
gradient. The fact that the real ionosphere had an even sharper
electric-field peak implies that the real ionosphere had a sharper

conductivity gradient than model run 1 (which is not surprising, in view of the gentle slopes in our model conductivities). The electric-field curves for runs 1 and 2 have smaller areas than those for run 4, because for run 4 the polar-boundary potential drop was substantially higher (see Table 2, Paper 1).

An important feature of our predicted Birkeland currents is that we get only downward currents in the subauroral region on the dusk side. Also, only downward currents are required for rapid subauroral flow in the Southwood-Wolf (1978) model. The data are in agreement with the model on this crucial point. (See panel 2 of Figure 12.)

On the other hand, there is a substantial and interesting quantitative disagreement between model and measured Birkeland currents for this pass, which implies that our first-try computer model, while in good agreement with data with regard to the rapid-subauroral-flow electric fields, has quantitative inaccuracies in other respects. We overestimated the total strength of Birkeland currents into, and just equatorward of, the rapid-flow region by almost a factor of 5. Because of the great smearing in our conductivity model, our model Pedersen conductivity in the rapid-flow region, while substantially smaller than at higher latitudes, is still ∼2 mhos, much higher than a realistic ionospheric-trough value. The actual ionospheric conductivity at the peak of the rapid flow can be estimated from the observed ratio $\Delta B_{west} / \mu_o E$, which, at the observed peak and for our assumed baseline for ΔB, is ∼ 0.3 mhos, a reasonable value for the trough. Figure 12, like most of the preceding five figures, indicates that the Birkeland currents exhibit more latitudinal spreading in reality than in the model,

as discussed in section III.

With regard to conductivity in the trough region, Banks and Yasuhara (1978) have recently pointed out that the strong electric field in a rapid-subauroral-flow region would rapidly deplete the supply of E-region ions and thus produce an anomalously low conductivity. The effect on the F-region is not clear, although Rich et al. (1980) have seen evidence of a tendency for the F-region to be depleted. However, as mentioned above, the ratio $\Delta B_{west}/\mu_o E$ at the observed peak suggests a height-integrated conductivity at that location that is a normal value for the ionospheric trough.

V. MODEL CURRENT SYSTEM

A. Summary Sketch

The standard magnetospheric-convection current system (see, e.g., Schield et al., 1969; Lyatsky and Maltsev, 1972; Sugiura, 1975; Wolf, 1974) is shown in Figure 13. Starting at the point S in the diagram, we have downward region-1 Birkeland current, westward and equatorward current in the dawn side of the auroral ionosphere, upward region-2 Birkeland current, westward partial-ring current around the night side of the magnetosphere, region-2 Birkeland current down to the duskside ionosphere, eastward and poleward current on the dusk side of the auroral ionosphere, upward region-1 Birkeland current to the magnetopause boundary layer and some sort of connection to the Chapman-Ferraro currents and/or solar wind.

B. Global Pattern of Birkeland Currents

Figure 14 shows one of our computed Birkeland-current distributions, in comparison with an observational summary diagram published by Iijima and Potemra (1978). The region-1 Birkeland currents lie just poleward of the boundary of our calculation. We estimate them by the simple assumption that horizontal currents flowing into or out of our poleward boundary are completed directly by Birkeland currents. That is, we neglect horizontal ionospheric currents flowing poleward of our boundary (at approximately 70°). In the diagram of model Birkeland currents, the latitudinal thickness of the region-1 Birkeland currents was chosen arbitrarily.

The theoretical and observational sides of Figures 14 agree with regard to general sense and pattern, which is not surprising, since convection theory predicted the general pattern (Schield et al., 1969;

Lyatsky and Maltsev, 1972; Vasyliunas, 1972; Wolf, 1974) before it was observed (Zmuda and Armstrong, 1974; Suguira, 1975).

We are encouraged by the fact that our more elaborate model now predicts a nightside overlap region that agrees qualitatively with observations. Moving equatorward from the polar cap near midnight, one encounters downward, upward, then downward currents, in either theory or observations. In the model, there are two competing parts of the region-2 Birkeland currents in the postmidnight sector. Energetic ions there (e.g., Figure 4d) connect to upward Birkeland currents, but low-energy ions (e.g., Figure 4a) and electrons, which come closer to the earth at dawn than at dusk and penetrate closer to the earth than the energetic ions in the postmidnight sector, connect to downward Birkeland currents, which predominate at the low-latitude edge of the auroral zone. Thus the observed Birkeland-current-overlap pattern can be explained simply in terms of the different shapes of the inner edges of energetic ions on the one hand, and low-energy ions and electrons on the other.

There is one obvious discrepancy between the theoretical and observational sides of Figure 14. Namely, the observational diagram is rotated eastward on the night side by ~ 2 hours local time. We assumed for simplicity that the potential at our poleward boundary was exactly antisymmetric about the noon-midnight meridian. Cowley (1973), McIlwain (1974) and others have argued in effect that the peak westward electric field at the polar-cap boundary occurs before midnight, and Figure 14 seems to confirm this. Because of Hall conductivity effects, a Birkeland-current pattern that is exactly antisymmetric about the

noon-midnight meridian corresponds to a potential pattern that does not

have the same antisymmetry, but is instead rotated. This conclusion is

implicit in the results of other models [Nopper and Carovillano, 1978;

Kamide and Matsushita, 1979a,b; Nisbet et al., 1978]. In future runs of

our simulation, we will concentrate on the westward electric field at the

polar boundary in the premidnight sector, to see if that does indeed

bring the model Birkeland-current pattern into better agreement with

Iijima and Potemra (1978).

C. Horizontal Ionospheric Currents

Figures 15-17 show the model pattern of horizontal current at a

particular time during the event. (The pattern is qualitatively similar

for all times.) The Hall current forms the standard eastward and

westward electrojets; the Pedersen current, which is comparable to the

Hall current in density, is poleward on the dusk side, equatorward on the

dawn side. The Pedersen currents are completed by Birkeland currents, as

shown schematically in Figure 13.

We wish to emphasize two points with regard to the

horizontal-current patterns shown in Figures 15-17:

(i) Except near noon and midnight, Pedersen currents are basically

meridional and Hall currents are basically azimuthal. Little current

flows equatorward of the plasma-sheet inner-edge region.

(ii) Although Hall-current density is typically a little larger than

Pedersen-current density, the total meridional Pedersen current on either

the dawn or the dusk side is larger than the azimuthal Hall current.

With regard to Point (i), we note that current patterns with these

characteristics have been derived on more observational grounds by

various authors. (See, e.g., Hughes and Rostoker, 1977; Volland, 1979).
Here we have demonstrated that the pattern is inherent in our model, in
which inner-magnetospheric and ionospheric currents are computed
self-consistently. The tendency for the inner edge of the
plasma-sheet/ring-current region to shield the low-latitude region from
the convection electric field causes the east-west electric field to be
small throughout most of the sunward-flow region. However, some of the
recent theoretical calculations based on TRIAD magnetometer measurements
(Yasuhara and Akasofu, 1977; Nopper and Carovillano, 1978; Gizler et al.,
1979) indicate quite substantial electric-field penetration to low
latitudes. In defense of our theoretical conclusion that the shielding
is generally good, we note the following:

(a) Chatanika measurements usually show a predominantly meridional
electric field in the diffuse aurora near dawn or dusk. (See, e.g.,
Horwitz et al. (1978).)

(b) There is generally good agreement between our theory and S3-2 data
with regard to the penetration of meridional electric fields to low
latitudes. (See Section III.)

(c) The azimuthal electric fields measured from S3-2 are generally tiny
compared to the meridional component in our modeled region, for orbits
4079A and B, except for the dawn side of orbit 4079A-north, through the
morning polar cusp. In this latter case, both model and data indicate
eastward electric field.

(d) Our computed east-west electric fields at $L \sim 4$ agree well with
whistler measurements averaged over many substorms. (See Paper 3.)

With regard to point (ii), we remark that, for the case shown in

Figures 15-17, the equatorward Pedersen current on the dawn side is ~3 x 10^6 amps, whereas the westward electrojet in the modeled region only totals about 2 x 10^5 amps. We estimate that a maximum of about 10^6 amps of westward electrojet flowed just poleward of our modeling region in the 19 September 1976 event. Still, it seems likely that the total equatorward Pedersen current on the dawn side usually exceeds the westward electrojet. Similarly, on the dusk side, the total poleward Pedersen current usually exceeds the eastward electrojet.

D. The Asymmetric ΔH at Low Latitudes During Magnetic Storms

Classic observations showed that the storm-time variation ΔH of the horizontal component of magnetic field at low latitudes has a systematic local-time dependence. Namely, the depression of H is greatest in the dusk-to-midnight sector; the local time of maximum |ΔH| is about 2200 MLT early in the main phase, and gradually moves to about 1800 MLT as the storm develops (Akasofu and Chapman, 1967). This characteristic asymmetry has often been interpreted in terms of a partial ring current centered at 1800-2200 MLT, and associated Birkeland currents. For an interesting and complete discussion of the classic work, see the review by Fukushima and Kamide (1973). A much briefer but more recent review is given by Nishida (1978).

Let us now consider this old asymmetric-ΔH problem from the point of view of our computer models. Consider the model event, which seems to

include the beginning of the injection of some ions into closed orbits, to form a trapped ring current. Figure 4 makes it clear that, throughout the event, the basic asymmetry of the ring current is such that the greatest strength is near midnight, minimum (actually zero) strength at noon; the strengths are approximately equal at dawn and dusk.

The top panel of Figure 18, which shows partial-ring-current strength as a function of local time at 1150 UT, exhibits the same approximate dawn-dusk symmetry. As discussed in subsection B above, our global model current pattern seems to be rotated by ~2 hours local time, relative to averaged observations. If we were to correct that as discussed earlier, by a change in boundary conditions at the polar cap, this would presumably produce a ring current with approximate symmetry about the 2200-1000 MLT meridian. However, this still doesn't seem consistent with the frequent observation of maximum $|\Delta H|$ near local dusk. Thus the simple interpretation of the observed asymmetry in terms of a single partial ring and associated Birkeland current is not quite adequate.

G. L. Siscoe and N. U. Crooker (private communication, 1978) have pointed out that the asymmetry in the low-latitude ΔH must be due either (a) to a Birkeland-current asymmetry with downward current near noon, upward current near midnight; or (b) to Hall currents flowing directly over the low-latitude stations (eastward on the dawn side, westward on the dusk side) (Siscoe, 1979). The asymmetric ring causes an asymmetric ΔH at the earth mainly indirectly, through its connections to Birkeland currents (Fukushima and Kamide, 1973).

Let us now consider mechanism (a) in the context of our model. Since

the region-1 Birkeland currents, which connect to solar wind and/or

outermost magnetosphere, are comparable to, and perhaps a bit larger

than, region-2 Birkeland currents, on the average, we should not neglect

region-1 Birkeland currents in discussing the asymmetry of ΔH.

Specifically, region-1 and region-2 currents generally oppose each other

[Iijima and Potemra, 1978], and it is therefore interesting to consider

the sum of the region-1 and region-2 currents, as a function of local

time. Such a plot based on our model is shown in the second panel of

Figure 18. The basic pattern is essentially independent of universal

time, although magnitudes and details vary. The crucial point is that

the model shows net downward Birkeland current near local noon and net

upward current on the night side, which would produce a negative ΔH on

the dusk side, positive ΔH on the dawn side.

In summary, we would expect the asymmetric part of the low-latitude

ΔH to consist of two parts: first, the magnetic field due to the sum of

region-1 and region-2 currents, which would cause maximum depression at

dusk, and an additional contribution due to the region-2 currents

(because they are closer to the low-latitude stations), which would cause

maximum depression near midnight. Detailed integrations of the

Biot-Savart law are in progress and will be reported in a future additional

paper. However, it appears that the observed asymmetry in low-latitude

ΔH can be reproduced approximately, despite the symmetry of the total

ring current about a meridian near noon-midnight.

Hughes and Rostoker (1977, 1979) earlier came to the conclusion that

the net Birkeland current is downward near noon. Their argument was

based on ground-magnetometer data, which can give an indication of the

sum R1+R2, and also on the fact that a net downward current is needed to
supply current to the eastward and westward electrojets, both of which
flow away from local noon. (See our Figure 15.) Our model calculation
clearly supports the results of Hughes and Rostoker (1977, 1979).

The third panel of Figure 18 shows Birkeland-current strengths vs.
local time, as derived from TRIAD data [Potemra, private communication,1979,
and Iijima and Potemra (1978)]. Although the observed and predicted
patterns of region-1 and region-2 currents agree rather well, as was the
case in Figure 14, the TRIAD data do not clearly show the theoretically
predicted net downward current in the noon region. Observational points
are missing near local noon, because the complex ΔB's observed by TRIAD
there are hard to resolve into "region-1" and "region-2" components.

Our theoretical model clearly indicates that a dawn-dusk asymmetry
in the low-latitude ΔH is due primarily to the asymmetry in net Birkeland
current, i.e., mechanism (a). In the model, mechanism (b) is of little
importance on the night side, where the low conductivity implies little
overhead current. On the day side, mechanism (a) and mechanism (b) are of
comparable importance, although mechanism (a) seems somewhat stronger, on
the average. The relative strengths of the two mechanisms depend on the
degree to which convection electric fields penetrate the shielding due to
region-2 Birkeland currents, a point we discussed in Section III and will
consider in more detail in Paper 3.

VI. JOULE HEATING AND RING-CURRENT ENERGY

A. Our Model Results

Since in our simulations, we compute partial ring currents and ionospheric currents and electric fields in a self-consistent manner, and since we have modeled the injection of a small ring current, we are in an ideal position to compare the amount of energy that is dissipated in Joule heating with the amount that goes into the ring current.

The total ring-current energy is given by

$$U_{ring} = \int_R u \, d^3x \qquad (2)$$

where u = internal energy of ring-current particles per unit volume and R = ring-current region. We take R to be our modeling region, which extends to $L \simeq 10$, and we sum over our 21 species.

The ring-current energy within a flux tube that has an equatorial cross section of unit area is given by

$$\sum_k [n_k(\int ds/B)^{-1}][\lambda_k(\int ds/B)^{-2/3}][B_e \int ds/B]$$

where the sum includes all species present in the flux tube, the first square-bracketed factor is the number density of species k in the flux tube, the second bracketed factor is the kinetic energy of a particle of species k, and the third bracketed factor is the flux-tube volume per unit area in the equatorial plane. The flux-tube volume integral extends from the southern ionosphere through the equatorial plane to the northern ionosphere. We thus write

$$U_{ring} = \sum_k n_k \lambda_k \int dA\, B_e\, (\int ds/B)^{-2/3} \qquad (3)$$

where the integral over A extends over the part of the modeled area of the equatorial plane that contains particles of species k. This area integral is approximated by an appropriate sum over grid points, with a first-order correction for finite radial grid spacing.

The total Joule heating is the integral of $\underline{j} \cdot \underline{E}$ over the ionosphere, which can be numerically approximated by a sum over our grid points.

$$JH = \sum_{hemispheres} \sum_{i,j} \Delta A \left[\underline{E}_h \cdot \left(\underset{\approx}{\Sigma} \cdot \underline{E}_h \right) \right] \qquad (4)$$

where ΔA, $\underline{E}_h$ and $\underset{\approx}{\Sigma}$ represent, respectively, the area, horizontal electric field and height-integrated conductivity associated with grid point (i,j).

Numerical values of U_{ring} and JH are plotted versus Universal Time in Figure 19, for two of our runs (1 and 4). The bottom panel gives the quotient JH/Φ_{pb}^2 , where Φ_{pb} is the potential drop across our polar boundary; the ratio JH/Φ_{pb}^2 represents the product of an effective conductivity and a geometrical factor. On the basis of the results in the fourth panel, we suggest that global Joule heating in the diffuse aurora and day side can be estimated by the formula

$$JH \sim (30 \text{ mhos})\, \Phi_{pb}^2 \qquad (5)$$

From Figure 19, the change in ring-current energy from 0900 to 1300 GMT

for run 1 is $\approx 1.4 \times 10^{15}$ J. The integrated Joule heating is given by

$$\int_{0900}^{1300} JH\ dt \approx 3 \times 10^{15}\ J \qquad (6)$$

so that

$$\frac{\int_{0900}^{1300} JH\ dt}{U_{ring}(1300) - U_{ring}(0900)} \approx 2.0 \qquad (7)$$

The corresponding ratio for run 4, representing a stronger-electric-field event, was 2.7. We thus find that most of the energy released in the event is dissipated as Joule heating.

The top two panels in Figure 19 suggest that the ratio of total Joule heating to ring-current energy depends on the length of time considered. Our conclusion that the Joule heating in our modeled region during an injection event is $\sim 2\ x$ (change in ring-current energy) depends on the idea that strong convection must be maintained for ~ 3 hours after onset to inject a significant ring current.

It should be emphasized that we have underestimated total global Joule heating by neglecting the region of the ionosphere poleward of the equatorward edge of the region-1 currents. Preliminary estimates [J. L. Karty, private communication, 1979] suggest that the Joule heating poleward of our boundary comprised $\sim 30\%$ of the global Joule heating in our modeled event. Thus our preliminary estimate of the global Joule heating including the polar region is ~ 3 times the change in ring-current energy for the modeled event. However, because Karty's estimate of the Joule heating poleward of our boundary on 19 September 1976 is

preliminary, and because we have no idea of how the ratio of polar to subpolar Joule heating varies from event to event, we will, in what follows, concentrate on the discussion of oule heating in our modeled region.

Since our estimate of the ratio of Joule heating to ring-current energy differs from many previous estimates, we should discuss the relationship between our result and previous ones, and also carefully explain and justify our answer.

B. Comparison with Previous Estimates

It has been known for a long time that Joule heating is an important source of energy for the thermosphere. (See, e.g., Cole (1975) or the recent review by Straus (1978).)

The Chatanika radar has been used extensively for measurement of Joule heating rates over the station, including the altitude profile of Joule heating (Brekke and Rino, 1978) and comparison of Joule heating with heating due to particle precipitation (Banks, 1977). In the cases studied by Banks (1977), Joule heating tended to be somewhat larger than heating by particle precipitation. Of course, it is difficult to derive global heating rates from a single incoherent-backscatter station.

Given the electric-field and neutral-wind distribution and ionospheric characteristics, one could straightforwardly calculate the global Joule heating rate; Volland (1979) has recently done this using a sophisticated semiempirical model of the global electric field, and his results are similar to ours in many respects. Specifically, he finds the diffuse-aurora and midlatitude regions to be very important, and his active-conditions model (Model II) yields a total heating rate similar to

the results shown in Figure 19. However, the problem we wish to address
here is that of estimating global Joule heating from parameters that can
be observed readily.

Let us begin by reviewing some earlier estimates of the global Joule
heating rate. Cummings and Dessler (1967) pointed out that substantial
Joule heating is implied by the idea that the ionosphere completes the
asymmetric ring current in the main phase of a geomagnetic storm. They
estimated that the total Joule dissipation involved was approximately
equal to the energy in the ring-current asymmetry. We have extended
their work in two major ways: (a) inclusion of the idea that a convection
electric field must exist in order to inject the ring current, and (b) quan-
titative integration of Joule heating over our modeled region. We consequently
derive about 2-3 times as large an estimate of Joule heating.

Similarly, Southwood (1977), in developing an analytic fluid model
of inner-magnetospheric convection, noted that a flux tube full of
ring-current particles traveling along the inner edge of the ring current
has its internal energy reduced by flux-tube expansion at a rate equal to
the Joule heating at its base. This does not address directly the
question of global Joule heating and, like the Cummings-Dessler result,
does not directly consider the injection.

The Cummings-Dessler and Southwood results, both based on
calculations of a partial ring completed through the ionosphere, suggest
a rough equipartition between ring-current energy and Joule heating. By
explicitly considering injection of the partial and full ring currents by
a convection eleccric field, we still have an order-of-magnitude

equipartition, but with Joule heating now dissipating 2-3 times as much energy as the ring current receives.

In contrast to these theoretical results, some observational arguments have indicated much smaller ratios of Joule heating to ring current energy. For example, Akasofu (1977) estimated that the ratio of Joule heating to ring current energy in a substorm was 0.07, forty times smaller than our estimate. However, Akasofu's estimate was based on Joule dissipation in the discrete-aurora region, which has smaller electric fields, on the average, and covers less area than the diffuse-auroral and subauroral regions that we consider. Akasofu (1977) also considers a shorter time period than we do (2 hours instead of 4). Integrating over much longer storm periods ($\approx$ 1 to 2 days), Perreault and Akasofu (1978) derive values near 0.2 for the ratio of Joule heating to ring-current energy.

C. Observational Estimate of Joule Heating/Ring Current

for 19 September 1976

The S3-2 data displayed in Figures 7-12 allow an approximate experimental check for our model Joule-heating rates. Namely, if we assume the Pedersen current to be meridional, and negligible at low latitudes, and if we neglect the divergence of the Hall current, we can say that the Pedersen current is approximately the ΔB plotted in Figures 7-12, divided by μ_o. To obtain the local Joule heating rate, we merely multiply by the observed E. We have done this for both theory (run 1) and observations in Figures 7-12, and have found that the model everestimates Joule heating by $\approx$ 15%, on the average, although individual passes are sometimes off by a substantial

factor. Thus the estimate given in equation 6 for the total Joule heating in our modeled region is probably approximately correct.

We can estimate the change in ring current during the event from Dst. The standard relation between the change in ring- current energy in a dipole field and magnetic perturbation ΔB at the equation is

$$\Delta B = -\frac{2}{3} B_0 \, (U_{ring}/U_m) \tag{8}$$

where $B_0 \cong 31{,}000\gamma$ (the field at the earth's equator), $U_m \cong 4\pi R_E^3 B_0^2/(3\mu_0)$ $= 8 \times 10^{17}$ joules (the total geomagnetic field energy external to the earth). (See, e.g., Cummings and Dessler (1967).) For our Olson-Pfitzer analytic-model magnetic field, which departs significantly from a dipole, we estimate that the factor 2/3 should be changed to approximately 0.45. Given that Dst dropped by about 14γ in the simulated event, we find from (8) that

$$U_{ring,max} \approx 8 \times 10^{14}\,\text{J} \tag{9}$$

The theoretical $U_{ring,\,max}$ value shown in Figure 10 is approximately equal to 1.75 times the value indicated in equation 9. We should also mention that the observed D_{st} recovered almost to its pre-substorm value for the hour 13-14 UT, a fact that is difficult to interpret within the model. In summary, for the 19 September 1976 event, the model tended to overestimate ring-current energy, and presumably to underestimate the ratio of Joule heating to ring current.

Incidentally, the S3-2 electron fluxes shown in Figures 4-6 of Paper 1 allow us to make a very rough estimate of the global energy deposition by electrons during the period 1000 UT - 1300 UT. If we make the very simple assumption that the energy deposition averaged over these

dawn-dusk passes equals the local-time-averaged energy deposition, we estimate a total energy in precipitated electrons equal to ~ 1.3×10^{14} J, less than one half of the estimated Joule heating in our modeled region (equation 6). Of course, much of the 1.3×10^{14} J energy associated with precipitating electrons was deposited poleward of our modeled region.

D. Analytic Argument

To indicate the generality of our result for the ratio of Joule heating to ring-current energy, we now use an analytic argument to estimate the same ratio.

The particle energy required to produce a partial ring current of strength J_p that goes halfway around the earth (as shown in the top half of Figure 20) is given by

$$U_{ring} = - \frac{3\Delta B U_m}{2B_0} = - \frac{3}{2} \left(- \frac{\mu_0 J_p}{4LR_E} \right) \frac{U_m}{B_0}$$

$$= \frac{3\mu_0 J_p}{8LR_E B_0} \left(\frac{4\pi}{3} R_E^3 \frac{B_0^2}{\mu_0} \right) = \frac{\pi}{2} \frac{B_0 R_E^2 J_p}{L} \tag{10}$$

where we have used equation 8.

Completion of this partial ring current is accomplished by ionospheric current, as indicated in the bottom half of Figure 20, and we must estimate the Joule dissipation involved. Half the partial ring current J_p is completed in each hemisphere. On each side of each hemisphere, $1/2\ J_p$ flows across half of the polar-boundary potential drop Φ_{pb}, so that

$$JH \sim \Phi_{pb}\ J_p \tag{11}$$

It takes ~ 3 hours for average ring-current particles to drift from local midnight to noon, and they must cross the critical region near noon if they are to form a complete ring. We thus find the following characteristic ratio

$$\frac{JH \cdot 3 \text{ hours}}{U_{ring}(t = 3 \text{ hours})} \sim 2 \left(\frac{L}{4}\right) \left(\frac{\Phi_{pb}}{100 \text{ kV}}\right) \qquad (12)$$

For our computer simulation, run 1 (Φ_{pb} = 80 kV and L $\sim$ 6), this formula gives a ratio of $\sim$ 2.4, in rough agreement with the ratio computed directly from the computer simulation.

It is not clear yet what fraction of the energy U_{ring} contained in the partial ring that exists 3 hours after onset could eventually form part of the complete symmetric ring. It is expected that future simulations will clarify the situation. However, it is hard to imagine U_{ring}(complete) > 2 U_{ring}(3 hours) unless there is a later substorm, and we shall simply assume that

$$U_{ring} \text{ (complete)} \sim U_{ring} \text{ (3 hours)}. \qquad (13)$$

Our essential result is this: if the ring current forms by means of a partial ring current, a part of which eventually drifts differentially around to make itself complete, then there is necessarily Joule dissipation associated with the ionospheric completion of the partial ring, dissipation that continues until the ring is complete. The only way we see to avoid theoretically the large Joule dissipation during ring-current injection would be to find a way to inject a ring current

symmetrically -- a theoretically difficult task that is complicated by the need to explain the asymmetries observed directly in the ring-current region, for example by Frank (1970) and Cahill and Lee (1975).

One must, of course, be somewhat cautious about deriving wide, general implications from the results of our simulation of the 19 September 1976 event. The simulated event was not strong enough to be classifiable as a full geomagnetic storm, and, for numerical-analysis reasons, we did not follow the model far enough to see a complete ring current form. In the actual 19 September 1976 event, Dst in fact recovered to its earlier value after a few hours, for reasons unknown. Until we successfully model a major geomagnetic storm, we won't be sure that we understand the essential physics of ring-current injection.

Nevertheless, the relatively high value we derive for the ratio of Joule heating to ring current energy has some support from thermospheric observations. Judging from the effect of a magnetic storm on the thermosphere, Hernandez and Roble (1978, 1979) have estimated that the energy received by the thermosphere during a storm correlates well with -d Dst/dt and that the total Joule heating appears to be of the same order of magnitude as the ring-current energy in such an event. This would be roughly consistent with our results. Tinsley (1979a, b) has proposed a reasonable alternative mechanism for dissipating part of the ring-current energy into the low- and mid-latitude thermosphere. However, if our results can be carried over in the obvious way to a geomagnetic storm, his mechanism would probably play a globally minor role in the thermospheric energy budget.

E. Simple Formulas for Estimating Global Joule Heating

Given the polar-boundary potential drop, one can estimate the global Joule heating in the diffuse aurora and day side from (5), which says that $JH \sim (30 \text{ mhos}) \, \phi_{pb}^2$. For average conditions, $\phi_{pb} \approx 50$ kV and

$$JH_{\text{region 2,average}} \sim 8 \times 10^{10} \text{ Watts} \tag{14}$$

The total global Joule heating should in principle·be somewhat greater than the values given by equation 5 or 14 or Figure 19, since we have excluded, in these estimates, most of the discrete aurora and the polar cusp.

If one extrapolates, to the case of a geomagnetic storm, our result that time-integrated Joule heating in our modeled region is about twice the change in ring-current energy, and relates U_{ring} to Dst using (8), one obtains

$$\left\langle JH_{\text{region 2}} \right\rangle \sim 2 \left\langle \frac{dU_{\text{ring}}}{dt} \right\rangle \sim (2 \times 10^{10} \text{ Watts}) \left\langle -\frac{dD_{st}}{dt} \right\rangle \tag{15}$$

where $dDst/dt$ is in gammas per hour and the brackets indicate an average over the period of ring-current injection (e.g., main phase). Formula (15) may be unreliable due to the great extrapolation involved, the considerable uncertainty in (8), and the difficulty of defining the period over which to average.

Perreault and Akasofu (1978) and Akasofu (1979) have used a different sort of formula for total Joule heating, namely

$$JH = (10^8 \text{ Watts}) \, AE_\gamma$$

where AE_γ is the AE index expressed in gammas. Based on the preliminary AE(5) index computed for 19 September 1976 [Van Sabben, 1977], we find that this AE-based formula gives a Joule-heating rate that is typically about 0.2 of the result shown in Figure 19 for run 1 (80 kV peak potential drop); of course, the Joule-heating results shown in Figure 19 should be underestimates, because they do not include Joule heating in

the high-latitude part of the electrojets and the main part of the polar cusp.

F. Final Comments on Joule Heating

We are irresistably tempted to use our initial model results as a basis for some comments on the general picture of energy transfer in the magnetosphere-ionosphere-atmosphere system, and on the specific matter of estimating the rate of energy transfer from the magnetosphere to the neutral atmosphere.

It is commonly thought that the solar-wind/magnetosphere system releases energy to the atmosphere primarily in brief but dramatic bursts called substorms. Our simulation results, and the extensive observational work on Birkeland currents and ionospheric electric fields over the last five years, suggest a subtly different picture, namely that energy is transferred from the solar wind and magnetosphere to the neutral atmosphere primarily by Joule heating, which occurs principally in the form of Pedersen currents through the polar-cusp, diffuse-aurora and ionospheric-trough regions. This type of Joule heating is perhaps better characterized as a convection phenomenon than as a substorm phenomenon. It occurs all the time, but at variable rate.

One cannot, of course, make a clear distinction between ionospheric-convection phenomena and substorm phenomena, because ionospheric convection and substorms must be correlated (Mozer, 1973). The correlation is, however, not very strong, and one leading observational study of the question failed to find any statistically significant relation (Heppner, 1973).

In our theoretical picture, the AE index, though convenient, is very

indirectly related to global Joule heating, since it measures essentially the peak strength of the Hall currents that make up the electrojets. Of course, it is the Pedersen currents that actually do the heating, not the Hall currents. Also, the AE index is not a direct index of electric fields and currents in the diffuse aurora and polar cusp, where, in our view, the majority of the Joule heating actually occurs. To improve observational knowledge of the energy transfer between the magnetosphere and ionosphere, we should improve monitoring of global magnetospheric convection by high-latitude radars and/or satellite measurements of the cross-polar-cap potential drop and Birkeland currents.

ACKNOWLEDGEMENTS

REFERENCES

Akasofu, S.-I., Physics of Magnetospheric Substorms, (D. Reidel) Dordrecht, Holland, p. 274, 1977.

Akasofu, S.-I., The solar wind-magnetosphere coupling and magnetospheric disturbances, preprint, 1979.

Akasofu, S.-I., and S. Chapman, A systematic shift of the DS axis, Planet. Space Sci., 15, 937, 1967.

Banks, P. M., Observations of Joule and particle heating in the auroral zone, J. Atm. Terrest. Physics, 39, 179, 1977.

Banks, P. M., and J. R. Doupnik, A review of auroral zone electrodynamics deduced from incoherent scatter radar observations, J. Atm. Terrest. Physics, 37, 951, 1975.

Banks, P. M., and F. Yasuhara, Electric fields and conductivity in the night-time E-region: a new magnetosphere-ionosphere-atmosphere coupling effect, Geophys. Res. Lett., 5, 1047, 1978.

Brekke, A., and C. L. Rino, High-resolution altitude profiles of the auroral zone energy dissipation due to ionospheric currents, J. Geophys. Res., 83, 2517, 1978.

Cahill, L. J., Jr., and Y. C. Lee, Development of four magnetic storms in February 1972, Planet. Space Sci., 23, 1279, 1975.

Cole, K. D., Energy deposition in the thermosphere caused by the solar wind, J. Atm. Terrest. Physics, 37, 939, 1975.

Cowley, S. W. H., A self-consistent model of a simple magnetic neutral sheet system surrounded by a cold, collisionless plasma, Cosm. Electrodyn., 3, 502, 1973.

Cummings, W. D., and A. J. Dessler, Ionospheric heating associated with the main-phase ring current, J. Geophys. Res., 72, 257, 1967.

DeForest, S. E., and C. E. McIlwain, Plasma clouds in the magnetosphere, J. Geophys. Res., 76, 3587, 1971.

Erickson, G. M., and R. A. Wolf, Is steady convection possible in the earth's magnetotail?, to be submitted to Geophys. Res. Lett., 1980.

Frank, L. A., Direct detection of asymmetric increases of extraterrestrial ring current proton intensities in the outer radiation zone, J. Geophys. Res., 75, 1263, 1970.

Fukushima, N., and Y. Kamide, Partial ring current models for worldwide geomagnetic disturbances, Rev. Geophys. Space Phys., 11, 795, 1973.

Gizler, V. A., V. S. Semenov, and O. A. Troshichev, Electric fields and currents in the ionosphere generated by field-aligned currents observed by TRIAD, Planet. Space Sci., 27, 223, 1979.

Harel, M., R. A. Wolf, P. H. Reiff, and M. Smiddy, Computer modeling of events in the inner magnetosphere, in Quantitative Modeling of the Magnetospheric Processes, Geophys. Monogr. Ser., vol. 21, edited by W. P. Olson, AGU, Washington, D. C., p. 499, 1979.

Harel, M., R. A. Wolf, P. H. Reiff, R. W. Spiro, W. J. Burke, F. J. Rich, and M. Smiddy, Quantitative simulation of a magnetospheric substorm, 1. Model logic and overview, to be submitted to J. Geophys. Res., 1980.

Heelis, R. A., R. W. Spiro, W. B. Hanson, and J. L. Burch, Magnetosphere-ionosphere coupling in the midlatitude trough, EOS (Trans. Am. Geophys. Un.), 57, 990, 1976.

Heppner, J. P., High-latitude electric fields and the modulations related to interplanetary magnetic field parameters, Rad. Sci., 8, 933, 1973.

Hernandez, G., and R. G. Roble, Relationship between midlatitude thermospheric winds and the time rate of change of Dst, Geophys. Res. Lett., 5, 835, 1978.

Hernandez, G., and R. G. Roble, On divergences of thermospheric meridional winds at midlatitudes, Geophys. Res. Lett., 6, 294, 1979.

Horwitz, J. L., J. R. Doupnik, P. M. Banks, Y. Kamide, and S.-I. Akasofu, The latitudinal distribution of auroral zone electric fields and ground magnetic perturbations and their response to variations in the interplanetary magnetic field, J. Geophys. Res., 83, 2071, 1978.

Hughes, T. J., and G. Rostoker, Current flow in the magnetosphere and ionosphere during periods of moderate activity, J. Geophys. Res., 82, 2271, 1977.

Hughes, T. J., and G. Rostoker, Comprehensive model current system for high latitude magnetic activity, 1. The steady state system, accepted for publication in Geophys. J. Roy. Astron. Soc., 1979.

Iijima, T., and T. A. Potemra, Large-scale characteristics of field-aligned currents associated with substorms, J. Geophys. Res., 83, 599, 1978.

Jaggi, R. K., and R. A. Wolf, Self-consistent calculation of the motion of a sheet of ions through the magnetosphere, J. Geophys. Res., 2852, 1973.

Kamide, Y., and S. Matsushita, Simulation studies of ionospheric electric fields and currents in relation to field-aligned currents, 1, Quiet periods, J. Geophys. Res., 84, 4083, 1979 a.

Kamide, Y., and S. Matsushita, Simulation studies of ionospheric electric fields and currents in relation to field-aligned currents, 2, substorms, J. Geophys. Res., 84, 4099, 1979 b.

Kelley, M. C., Evidence that auroral-zone electric fields act in opposition to super-rotation of the upper atmosphere, Planet. Space Science, 24, 355, 1976.

Kivelson, M. G., S. M. Kaye, and D. J. Southwood, The physics of plasma-injection events, paper presented at the AGU Chapman Conference on Magnetospheric Substorms and Related Plasma Processes, Los Alamos, New Mexico, October 1978 and to be published in Astrophysics and Space Science Library Series, 1979.

Konradi, A., C. L. Semar, and T. A. Fritz, Injection boundary dynamics during a geomagnetic storm, J. Geophys. Res., 81, 3851, 1976.

Lyatsky, W. B., and Yu. P. Mal'tsev, Three-dimensional current system of magnetic substorms, in Geophysical Investigations of Auroral Zone, Polar Geophysical Institute, Academy of Sciences, USSR, Apatity, pp. 74-86, 1972.

Lyons, L. R., and D. J. Williams, A source for the geomagnetic storm main phase ring current, submitted to J. Geophys. Res., 1979.

McIlwain, C. E., Substorm injection boundaries, in Magnetospheric Physics, edited by B. M. McCormac, D. Reidel, Dordrecht-Holland, p. 143, 1974.

Maynard, N. C., On large poleward-directed electric fields at sub-auroral latitudes, Geophys. Res. Lett., 5, 617, 1978.

Mozer, F. S., On the relationship between the growth and expansion phases of substorms and magnetospheric convection, J. Geophys. Res., 78, 1719, 1973.

Nisbet, J. S., M. J. Miller and L. A. Carpenter, Currents and electric fields in the ionosphere due to field-aligned auroral currents, J. Geophys. Res., 83, 2647, 1978.

Nishida, A., Geomagnetic Diagnosis of the Magnetosphere, Springer-Verlag, New York, p. 159ff, 1978.

Nopper, R. W., Jr., and R. L. Carovillano, Polar equatorial coupling during magnetically active periods, Geophys. Res. Lett., 5, 699, 1978.

Perreault, P., and S.-I. Akasofu, A study of geomagnetic storms, Geophys. J. R. Astr. Soc., 54, 547, 1978.

Rich, F. J., M. Smiddy, W. J. Burke, and D. A. Hardy, Observations of field-aligned currents in association with strong convection electric fields in the trough, to be published in J. Geophys. Res., 1980.

Roederer, J. G., and E. W. Hones, Jr., Motion of magnetospheric particle clouds in a time-dependent electric field model, J. Geophys. Res., 79, 1432, 1974.

Rostoker, G., and R. Boström, A mechanism for driving the gross Birkeland current configuration in the auroral oval. J. Geophys. Res., 81, 235, 1976.

Schield, M. A., J. W. Freeman, and A. J. Dessler, A source for field-aligned currents at auroral latitudes, J. Geophys. Res., 74, 247, 1969.

Siscoe, G. L., paper presented at the Workshop on the Geomagnetic Field, held at U. S. Air Force Geophysics Laboratory, Bedford, Massachusetts, April 1979.

Smiddy, M., M. Kelley, W. Burke, F. Rich, R. Sagalyn, B. Shuman, R. Hays, and S. Lai, Intense poleward-directed electric field near the ionospheric projection of the plasmapause, Geophys. Res. Lett., 4, 543, 1977.

Smith, P. H., and R. A. Hoffman, Direct observations in the dusk hours of the characteristics of the storm time ring current particles during the beginning of magnetic storms, J. Geophys. Res., 79, 966, 1974.

Southwood, D. J., The role of hot plasma in magnetospheric convection, J. Geophys. Res., 82, 5512, 1977.

Southwood, D. J., and R. A. Wolf, An assessment of the role of precipitation in magnetospheric convection, J. Geophys. Res., 83, 5227, 1978.

Spiro, R. W., W. B. Hanson, D. L. Sterling, and R. A. Hoffman, Midlatitude trough characteristics as observed by Atmospheric Explorer, EOS, Trans. Am. Geophys. Un., 58, 1159, 1974.

Spiro, R. W., M. Harel, R. A. Wolf, and P. H. Reiff, Quantitative simulation of a magnetospheric substorm, 3. Plasmaspheric electric fields and evolution of the plasmapause, to be submitted to J. Geophys. Res., 1980.

Spiro, R. W., R. A. Heelis, and W. B. Hanson, Ion convection and the formation of the midlatitude F-region ionization trough, J. Geophys. Res., 83, 4255, 1978.

Straus, J. M., Dynamics of the thermosphere at high latitudes, Rev. Geophys. Space Phys., 16, 183, 1978.

Sugiura, M., Identifications of the polar cap boundary and the auroral belt in the high-latitude magnetosphere: a model for field-aligned currents, J. Geophys. Res., 80, 2057, 1975.

Tinsley, B. A., Energetic neutral atom precipitation as a possible source of midlatitude F region winds, Geophys. Res. Lett., 6, 291, 1979a.

Tinsley, B. A., Energetic neutral atom precipitation during magnetic storms: optical emission, ionization, and energy deposition at low and middle latitudes, J. Geophys. Res., 84, 1855, 1979b.

Van Sabben, B., editor, IAGA Bulletin 32G, 1977.

Vasyliunas, V. M., The interrelationship of magnetospheric processes, in Earth's Magnetospheric Processes, edited by B. M. McCormac, D. Reidel, Dordrecht-Holland, p. 29, 1972.

Volland, H., Semiempirical models of magnetospheric electric fields, in Quantitative Modeling of the Magnetospheric Processes, Geophys. Monogr. Ser., vol. 21, edited by W. P. Olson, AGU, Washington, D. C., p. 261, 1979.

Wolf, R. A., Effects of ionospheric conductivity on convective flow of plasma in the magnetosphere, J. Geophys. Res., 75, 4677, 1970.

Wolf, R. A., Calculations of magnetospheric electric fields, in Magnetospheric Physics, edited by B. M. McCormac, D. Reidel, Dordrecht-Holland, p. 167, 1974.

Wolf, R. A., and M. Harel, Dynamics of the magnetospheric plasma, paper
    presented at the Chapman Conference on Magnetospheric Substorms and
    Related Plasma Processes, Los Alamos, New Mexico, October 1978,
        published in Astrophysics and Space Science Library Series, p.143,
    1979.

Yasuhara, F., and S.-I. Akasofu, Field-aligned currents and ionospheric
    electric field, J. Geophys. Res., 82, 1279, 1977.

Zmuda, A. J., and J. C. Armstrong, The diurnal flow pattern of
    field-aligned currents, J. Geophys. Res., 79, 4611, 1974.

TABLE 1.

Comparison of Predicted and Observed Strengths of ΔB's due to
Region-1 Birkeland Currents

Pass	$\Delta B_{predicted}$ (γ)	$\Delta B_{observed}$ (γ)
4079A-South-Dawn	170	230
4079A-South-Dusk	490	340
4079A-North-Dusk	600	370
4079A-North-Dawn	1060	640
4079B-South-Dawn	510	400
4079B-South-Dusk	590	720

50

FIGURE CAPTIONS

Figure 1. Custer's Last Stand (W. H. Campbell, private communication).
The figure shows total electric fields in the equatorial
plane, for 1050 UT, run 1. (The runs are described in Table 2
of paper 1.) The sun is to the left.

Figure 2. Total E x B-drift velocity in the equatorial plane, for 1050
UT, run 1.

Figure 3. Induction electric field at 1010 UT, for runs 1, 2 or 4.

Figure 4. (a) Time evolution of the inner edge of the ion plasma sheet
for low-energy ions, run 1. The magnetospheric
equatorial plane is shown. The ions have $\lambda = 478$ eV
$R_E^{2/3} \gamma^{-2/3}$, corresponding to $\approx$ 3 keV at L = 6.6. The
"U" and "D" symbols indicate connection of the inner edge
for 1300 UT to currents UP from the ionosphere and DOWN
into the ionosphere, respectively.

(b) Same as 4a, but for $\lambda = 1730$ eV $R_E^{2/3} \gamma^{-2/3}$,
corresponding to $\approx$ 12 keV at L = 6.6.

(c) Same as 4a, but for $\lambda = 3880$ eV $R_E^{2/3} \gamma^{-2/3}$,
corresponding to $\approx$ 27 keV at L = 6.6.

(d) Same as 4a, but for $\lambda = 8650$ eV $R_F^{2/3} \gamma^{-2/3}$,
corresponding to $\approx$ 60 keV at L = 6.6. The x's on the
curves for 1150 and 1300 UT indicate segments of the

computed curve that are artifacts of the numerical
method. The curve with circles on it indicates our guess
as to the true form of the curve near local noon for 1300
UT.

Figure 5. Geocentric distance of Alfvén layers and inner edges, for a
grid line at approximately 1820 MLT, for several universal
times during the event. The nonlinear abscissa shows energy
invariant, λ, while the ordinate shows geocentric distance in
earth radii. Error bars indicate regions of closed eddies of
plasma -- eddies that do not extend to the tail or magnetopause
and do not encircle the earth.

Figure 6. Ion arrival times at $L = 6.6$, 1820 MLT, for runs 1 - 4. The
x's give energies of the inner edge, for those ion species
that we follow in detail and are present at $L = 6.6$, MLT =
1820. Solid lines represent the lowest and highest energies
for which plasma-sheet ions should be present at that point.
The dotted curve represents the time that would be required
for such ions to simply gradient drift from local midnight.

Figure 7. Comparison of theory and data for the southern-hemisphere,
dawnside auroral portion of S3-2 orbit 4079A, which occurred
$\approx$9 minutes before substorm onset. The upper panel compares the
backward (roughly equatorward) component of observed electric
field with the +I (essentially equatorward) component of the

model electric field (run 1). The second panel compares the
observed ΔB with the modeled one, computed from equation 1.
Scales at the bottom show degrees invariant latitude from the
boundary of the calculation; satellite invariant latitude and
magnetic local time; and Greenwich Mean Time in hours:
minutes: seconds, and also seconds. Satellite altitude was
approximately 1025 km. Theoretical curves are for 1010 UT and
for a grid line at approximately 4.8 MLT. The nominal model
polar-cap invariant latitude was 71.24°.

Figure 8. Comparison of theory and data for the southern-hemisphere
duskside auroral portion of orbit 4079A, which occurred ≈ 9
minutes after substorm onset. The upper panel compares the
backward (≈ poleward) component of the observed E with the -I
(≈ poleward) component of theoretical E's (for run 1, and for
runs 2 and 4, which are identical for this UT). The format is
otherwise the same as Figure 7. Satellite altitude was
approximately 1375 km. Theoretical curves are for 1010 UT and
for a grid line at approximately 19.2 MLT. Nominal model
polar-cap invariant latitude was 71.24°.

Figure 9. Comparison of theory and data for the northern-hemisphere
duskside auroral portion of orbit 4079A, which occurred about
the time of peak electrojet activity. The upper panel
compares the forward (≈ poleward) component of the observed E
with the -I (≈ poleward) component of the theoretical E's (for

run 1, and for runs 2 and 4, which are identical for this UT). The format is otherwise similar to Figure 7. Satellite altitude was approximately 600 km. Theoretical curves are for 1040 UT and for a grid line at approximately 17.5 MLT. Nominal model polar-cap invariant latitude was 72.12°.

Figure 10. Comparison of theory and data for the northern-hemisphere dawnside auroral portion of orbit 4079A, which occurred about the time of peak electrojet activity. The upper panel compares the forward ($\approx$ equatorward) component of the observed E with the +I ($\approx$ equatorward) component of the theoretical E's (for runs 1 and 4). The format is otherwise similar to Figure 7. Satellite altitude was approximately 264 km. Theoretical curves are for 1130 UT and for a grid line at approximately 9.2 MLT. Nominal model polar-cap invariant latitude was 73.23°.

Figure 11. Comparison of theory and data for the southern-hemisphere dawnside auroral portion of orbit 4079B, which occurred about 90 minutes after onset. The format is similar to Figure 7, but results are shown for runs 1 and 4. Satellite altitude was approximately 1020 km. Theoretical curves are for 1130 UT and for a grid line at approximately 6.5 MLT. Nominal model polar-cap invariant latitude was 72.12°.

Figure 12. Comparison of theory and data for the southern-hemisphere duskside auroral portion of orbit 4079B, which occurred about 110 minutes after onset. The format is similar to Figure 8, except that results from runs 2 and 4 are presented separately, and model height-integrated Pedersen conductivities are shown in a fourth panel. Satellite altitude was approximately 1370 km. Theoretical curves are for 1150 UT and a grid line at approximately 19.2 MLT. Nominal polar cap invariant latitude was 71.26°.

Figure 13. Schematic diagram of the basic magnetospheric-convection current system. The three-dimensional distribution of currents, which in our computer model is approximated by about 3400 wires, is shown schematically as a few thin wires. The view is from behind (antisunward) of the earth, and above the equatorial plane. The lined region is the equatorial plane; the dotted region, the dayside magnetopause. The notations "R1", "R2" and "PRC" mean "Region-1 Birkeland Current", "Region-2 Birkeland Current" and "Partial Ring Current".

Figure 14. Comparison of a typical computed Birkeland-current pattern (1150 UT, run 1) and an average observed pattern for active times (Iijima and Potemra, 1978).

Figure 15. Density of height-integrated Hall current, for 1150 UT, run 1. The concentric circles are at 10° intervals in invariant latitude.

Figure 16. Density of height-integrated Pedersen current, for 1150 UT, run 1. The concentric circles are at 10° intervals in invariant latitude.

Figure 17. Density of height-integrated total current, for 1150 UT, run 1. The concentric circles are at 10° intervals in invariant latitude.

Figure 18. (a) Model partial ring current crossing various local times, in units of 10^6 Amps (MA), for 1150 UT, run 1.

(b) Predicted Birkeland current per unit local time per hemisphere, for 1150 UT, run 1. Here "R1", "R2" and "R1 + R2" refer, respectively, to region-1 current, region-2 currents, and net Birkeland current. Current is given in units of kiloamps per hour of local time. Upward current out of the ionosphere is positive. Diagram (a) is essentially twice the integral of the R2 curve in Diagram (b).

(c) Average observed Birkeland current per hour local time, for $|AL| \geq 100$ γ. Derived from Potemra (private communication) and Iijima and Potemra (1978).

Figure 19. Ring current energy and Joule heating as a function of Universal Time through the event. Results are shown for runs 1 and 4. The bottom panel shows the ratio of Joule heating to the square of the polar-boundary potential drop.

Figure 20. Qualitative diagram of partial ring current during injection
(top diagram) and corresponding ionospheric current (bottom
diagram).

CASE 1 TOTAL ELECTRIC FIELD INCLUDING COROTATION   IC=11
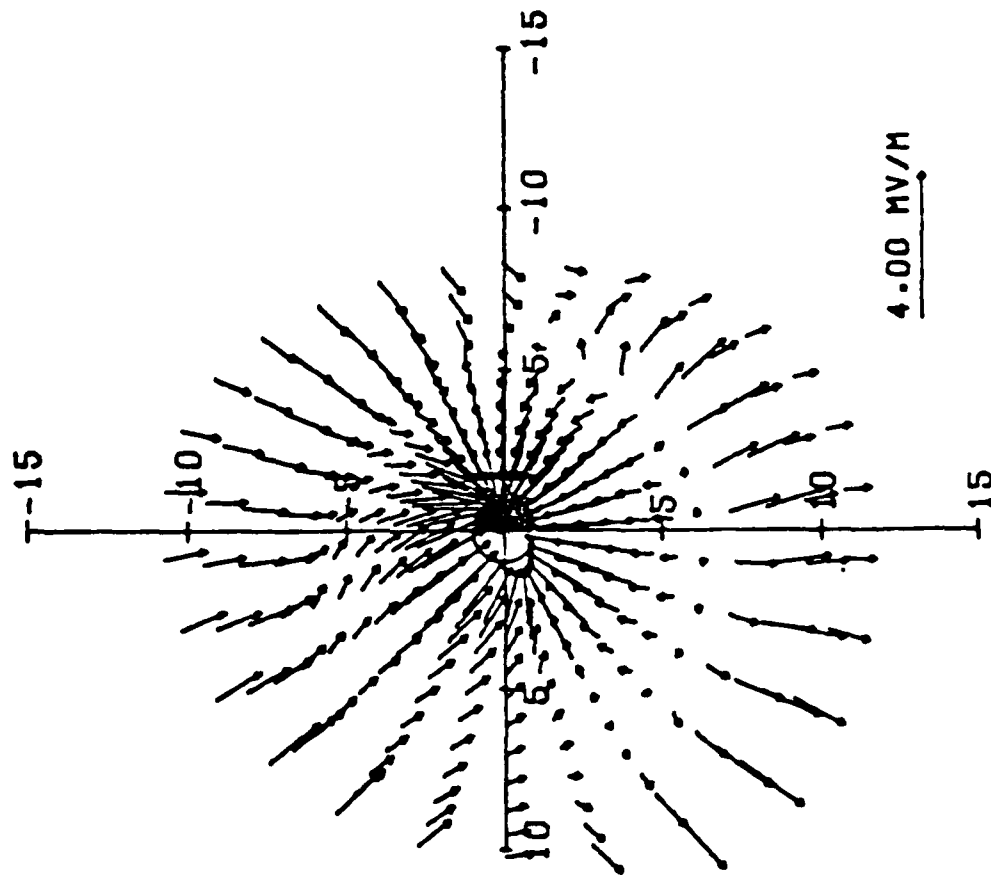
TIME = 10:50

Figure 1

CASE 1 TOTAL VELOCITY FLOW FIELD   EQUATORIAL PLANE   IC=11

TIME = 10:50

28.00 KM/SEC
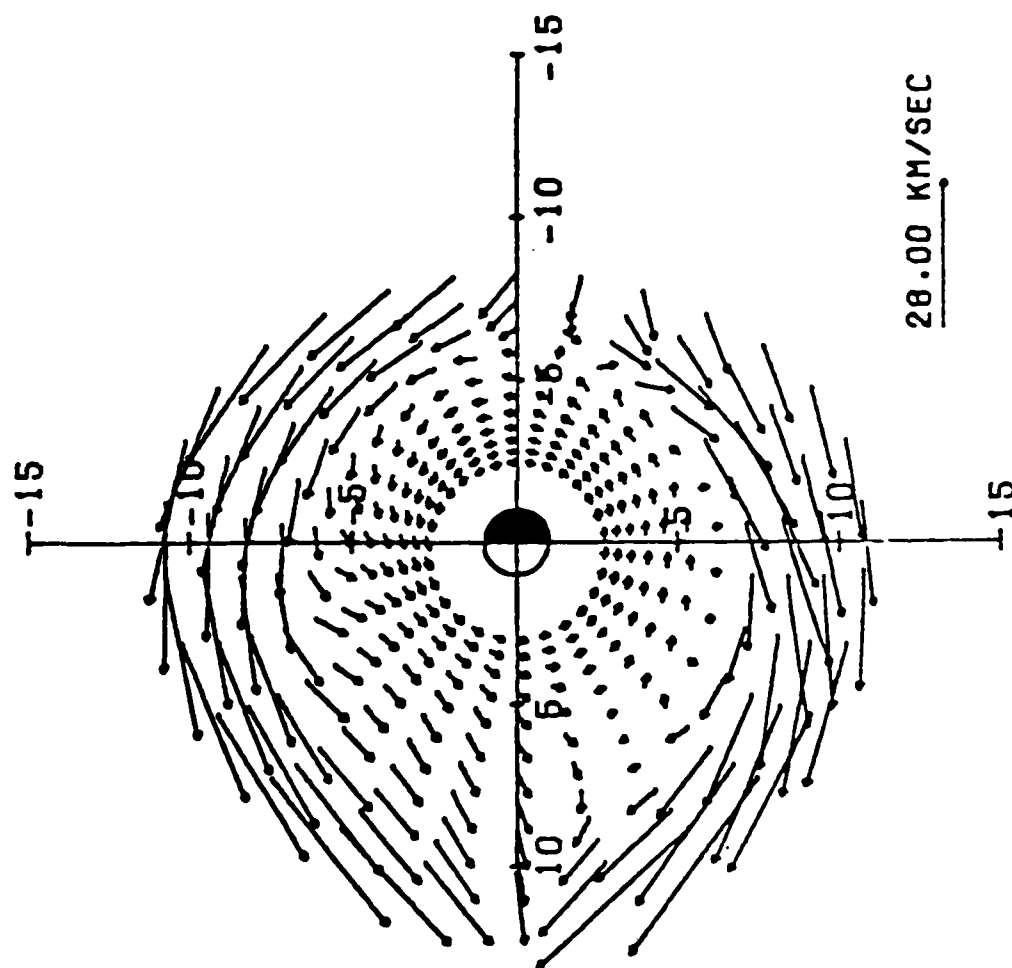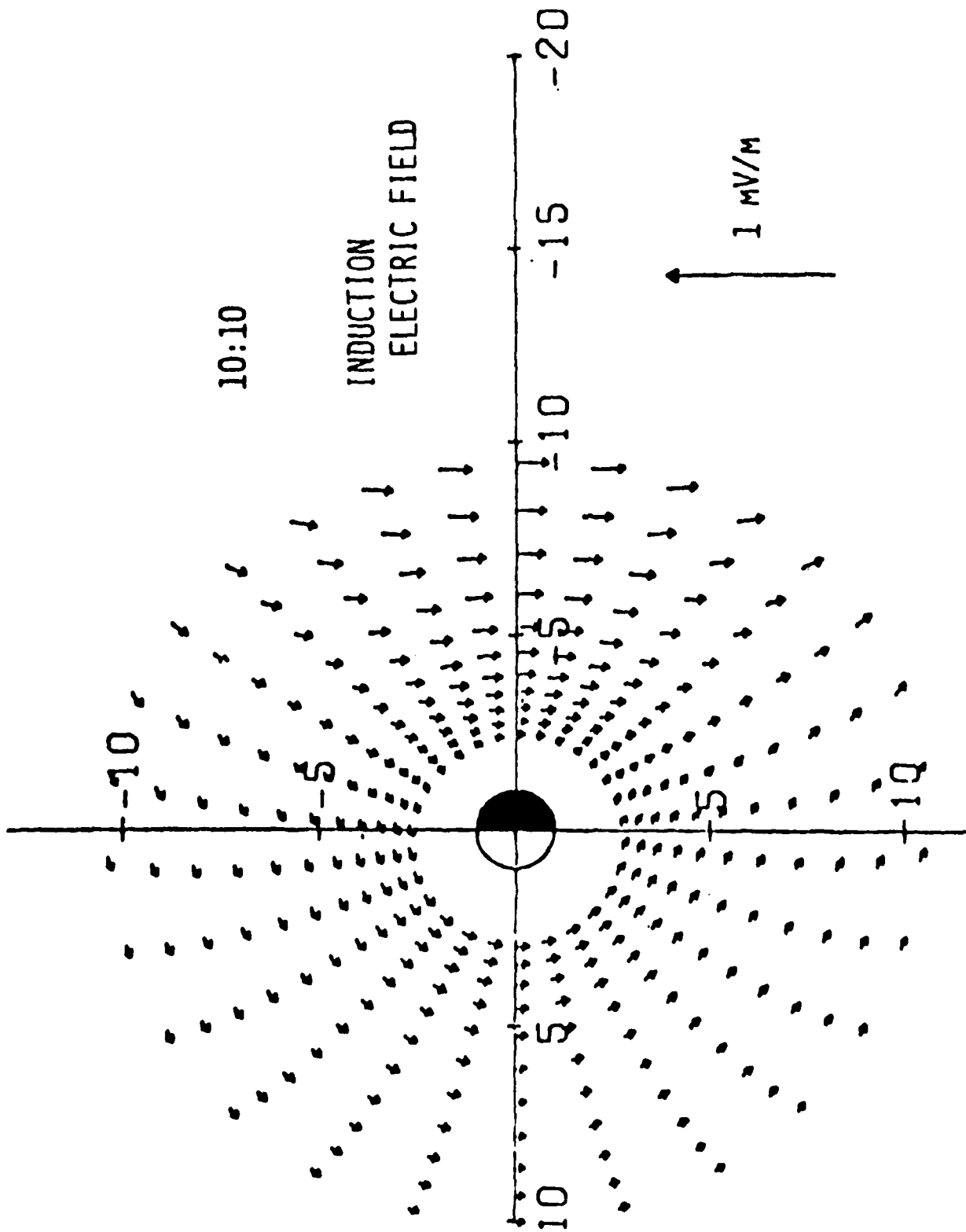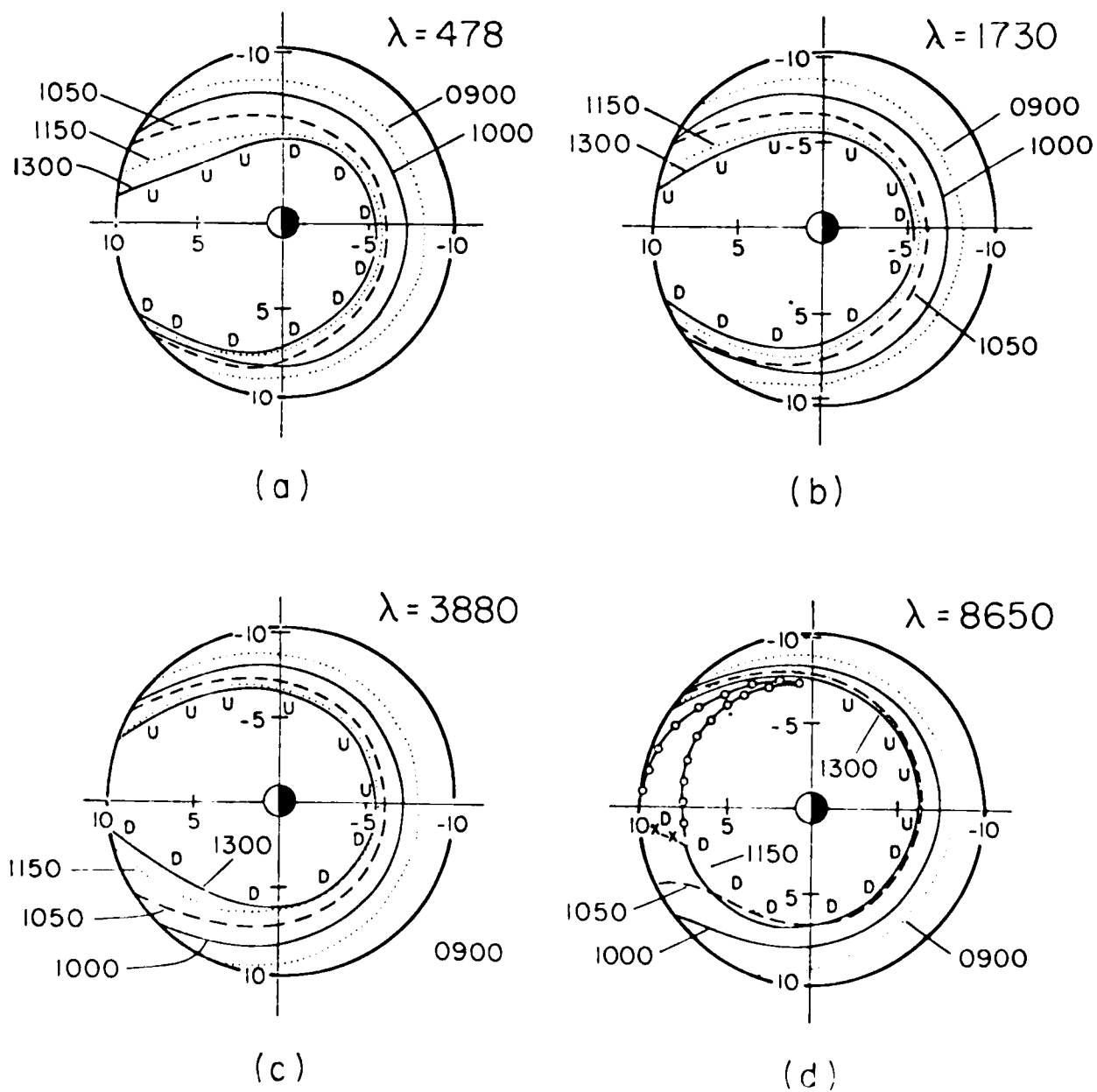
Figure 2

Figure 3

Figure 4
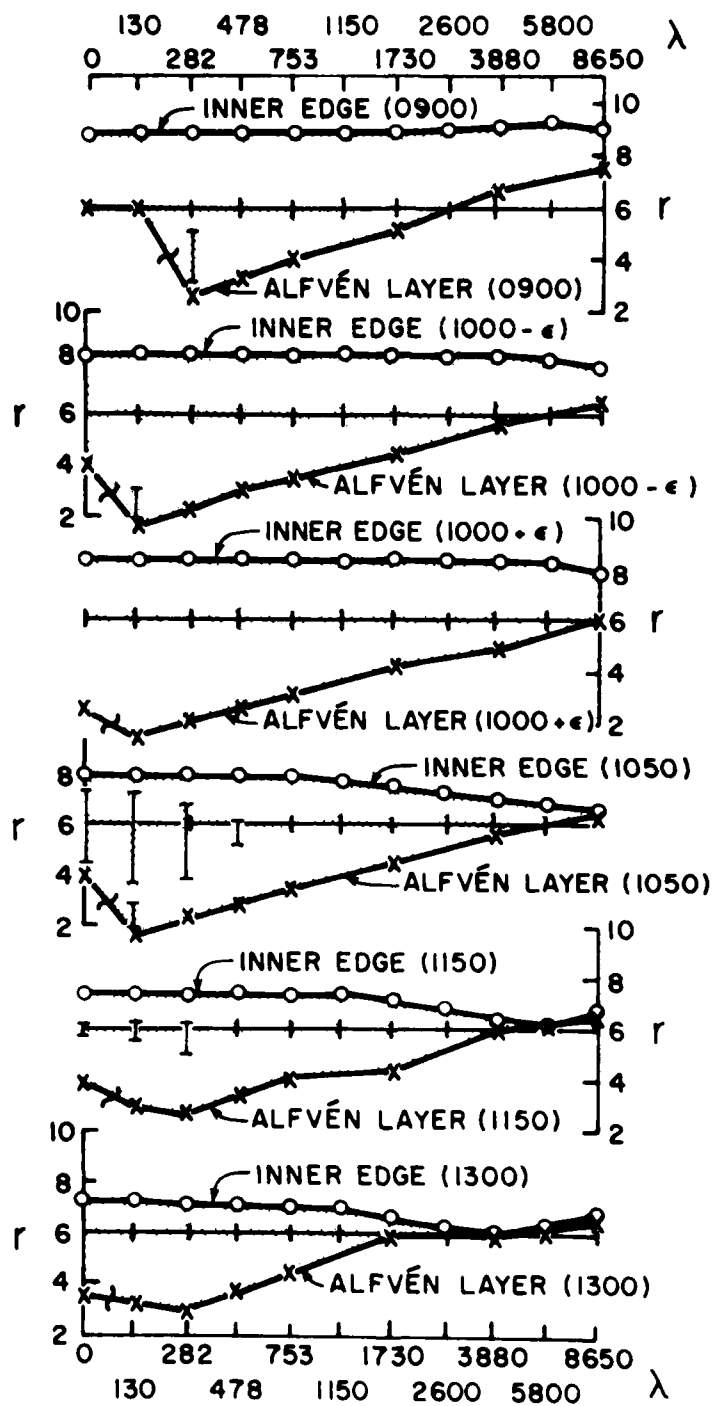
Figure 5
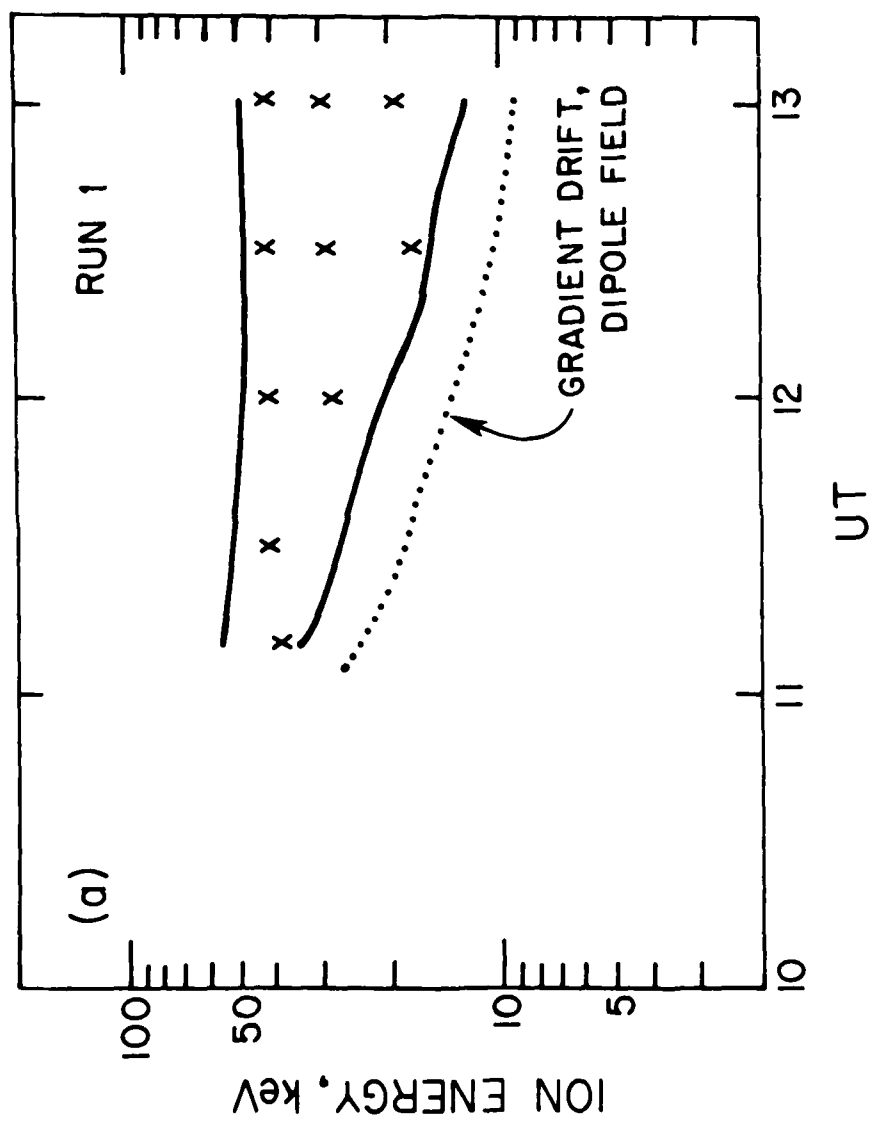
Figure 6a
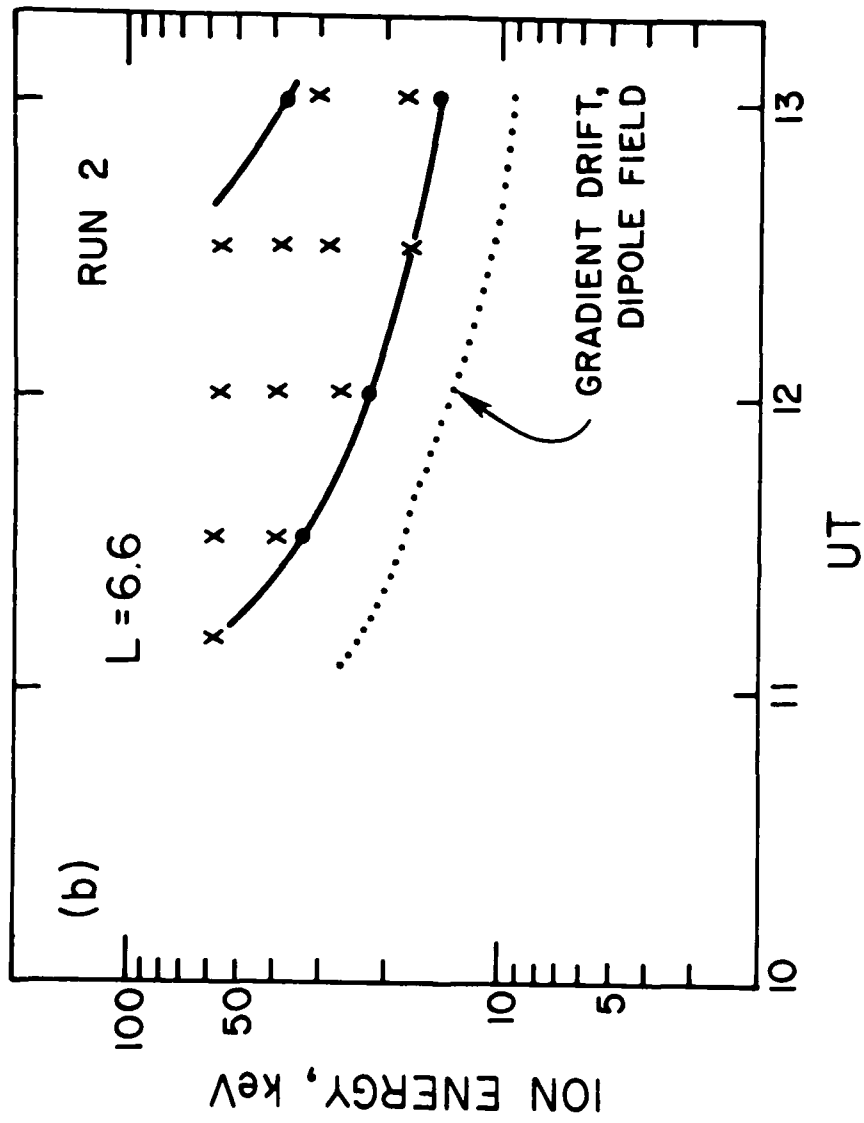
Figure 6b
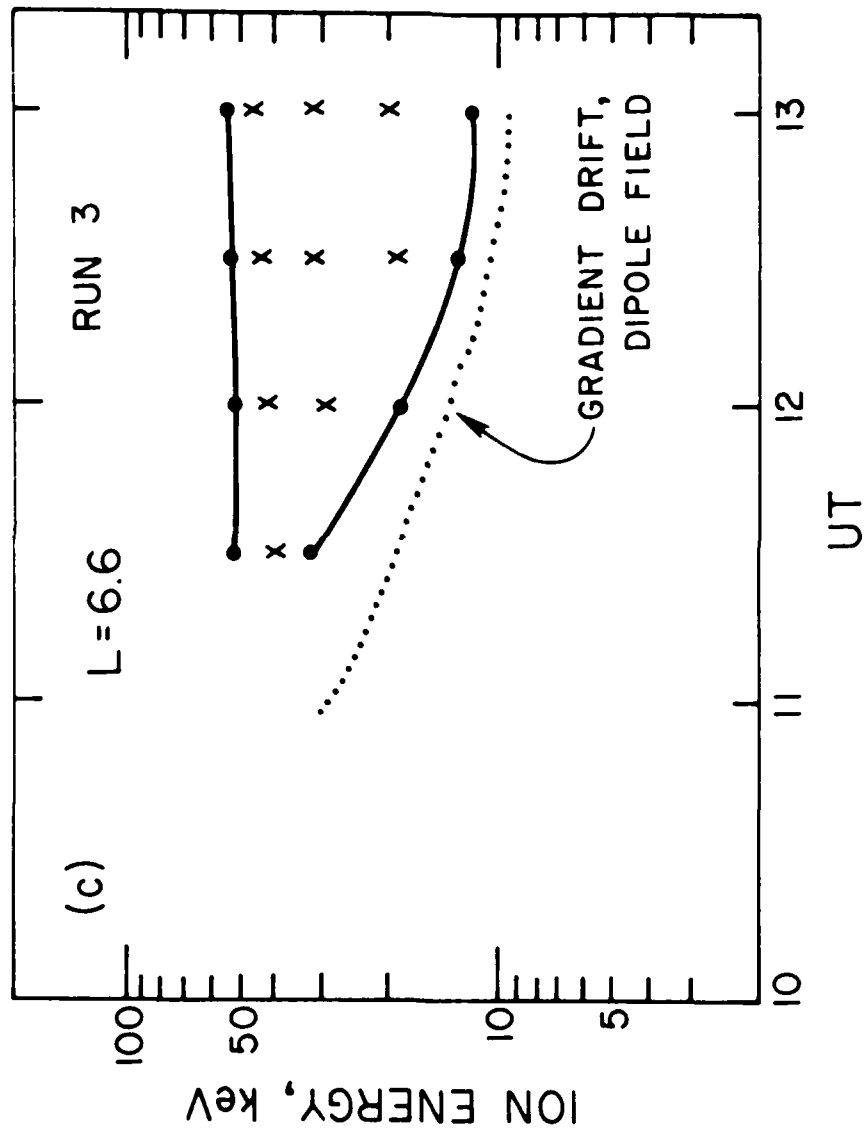
Figure 6c

Figure 6d

66
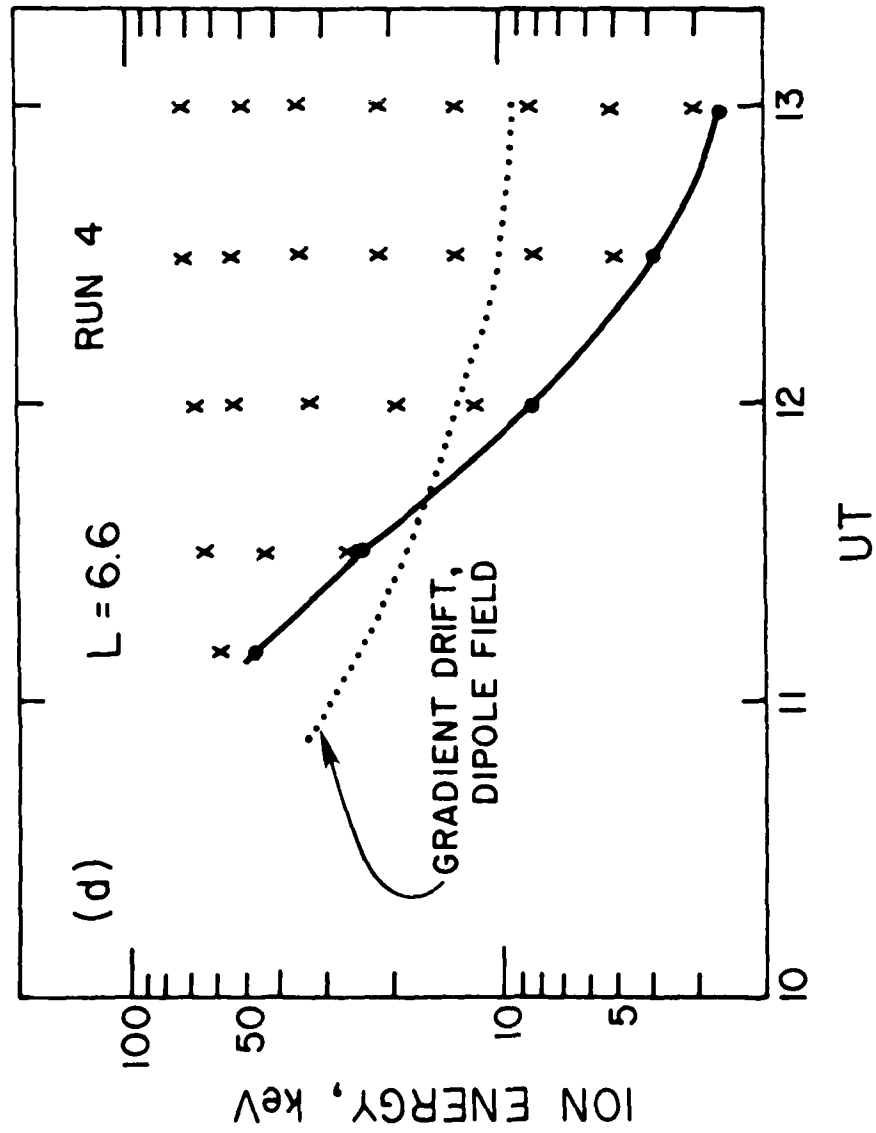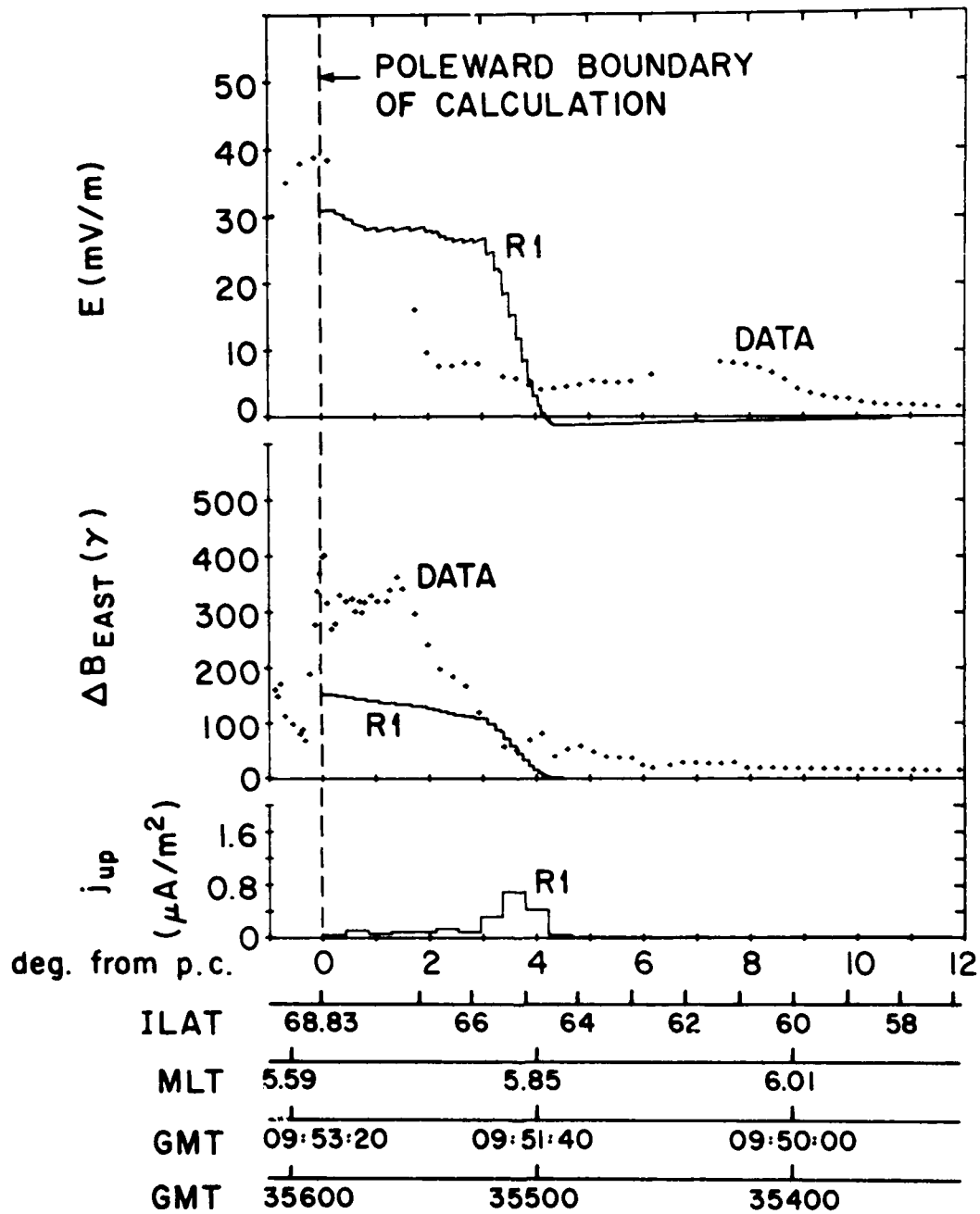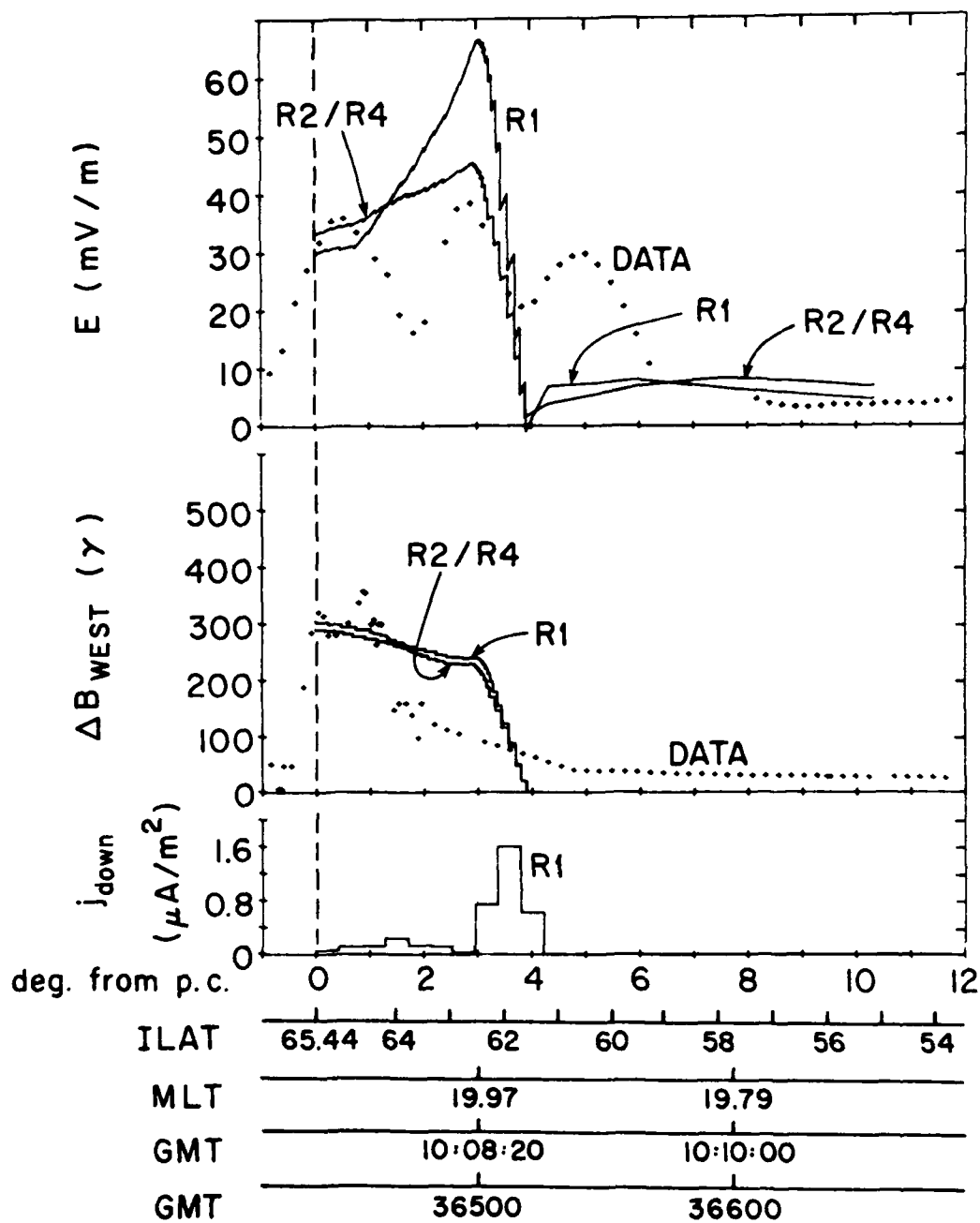
Figure 7

Figure 8

68
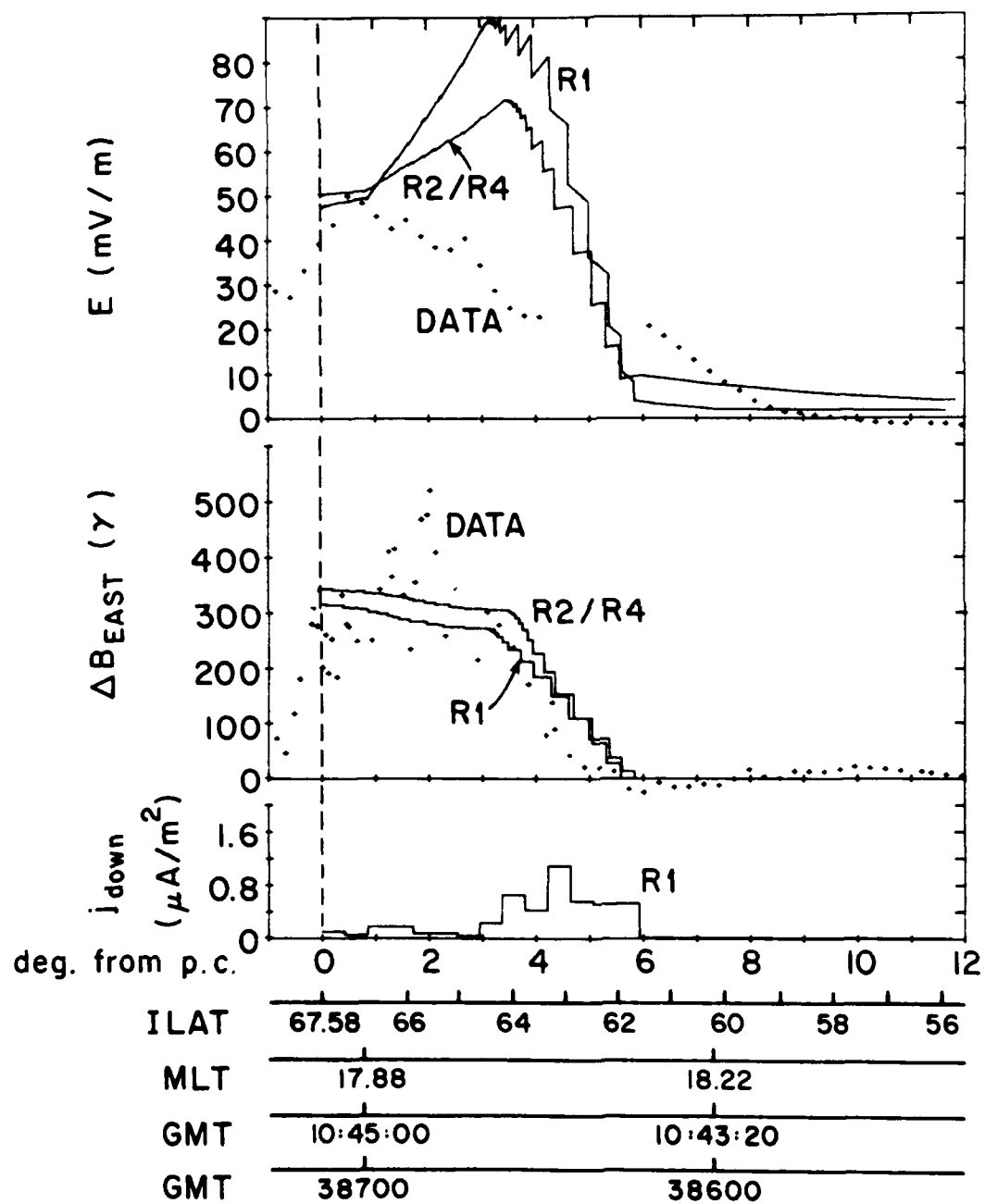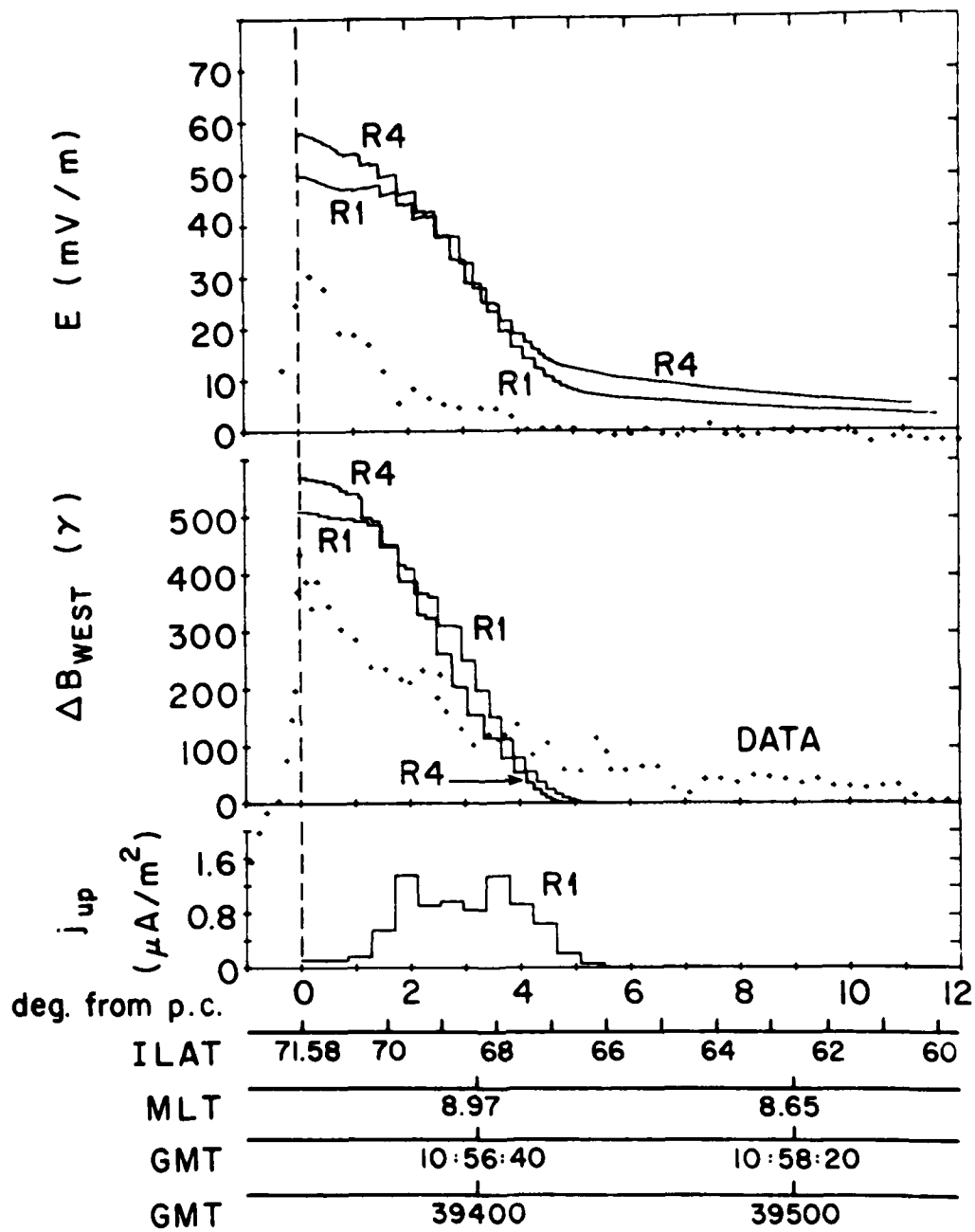
Figure 9

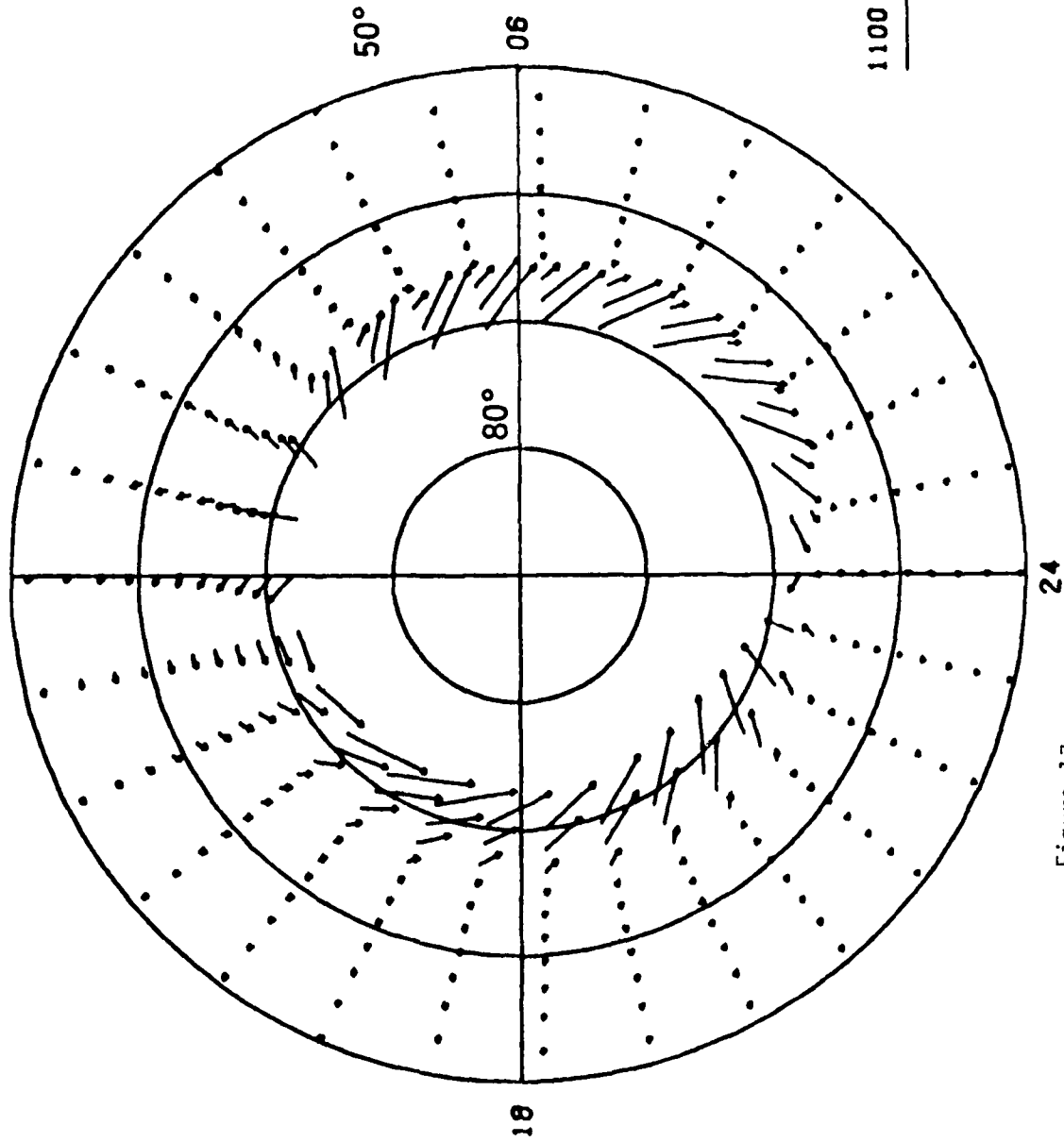Figure 10
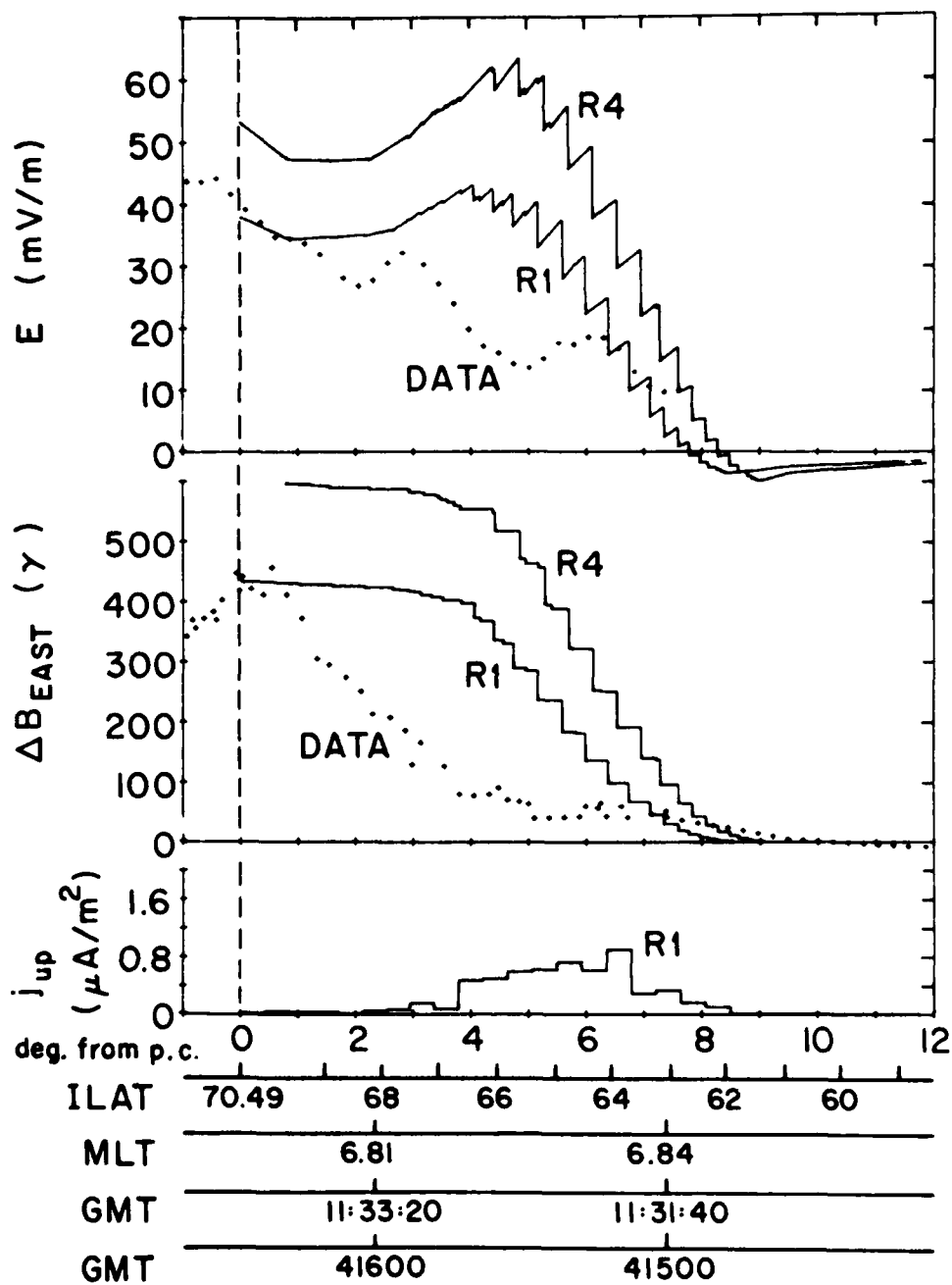
Figure 11
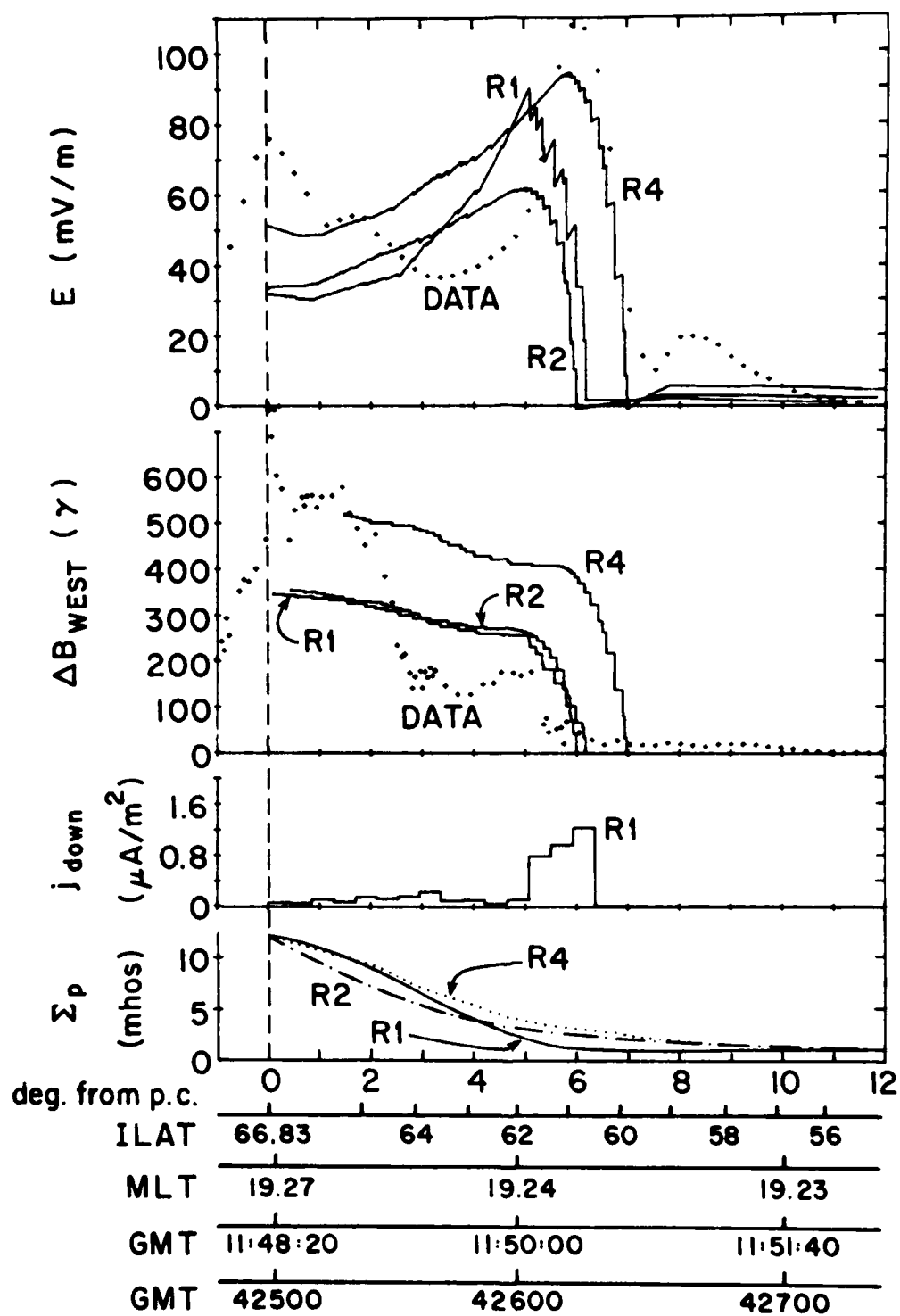
Figure 12
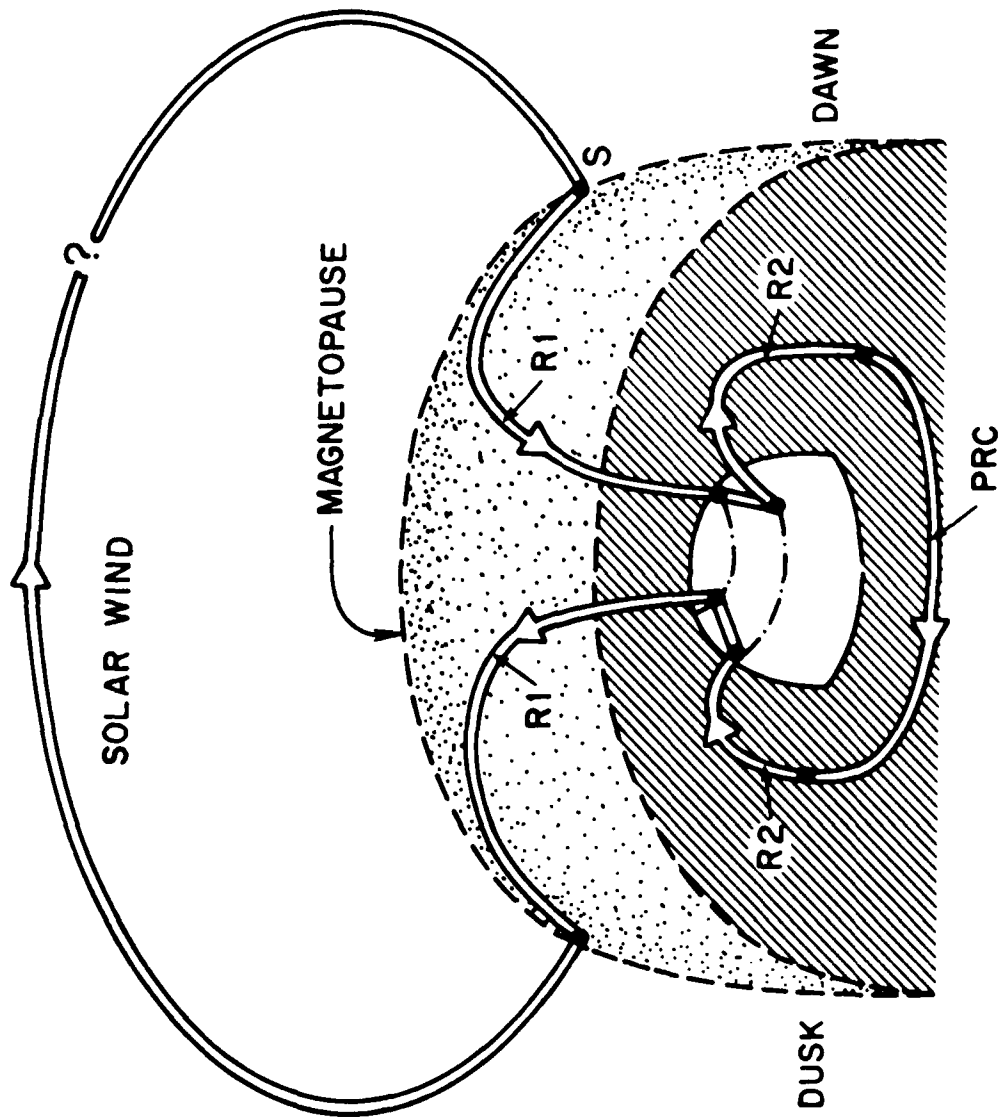
Figure 13

OBSERVATION

$|AL| \geq 100\gamma$
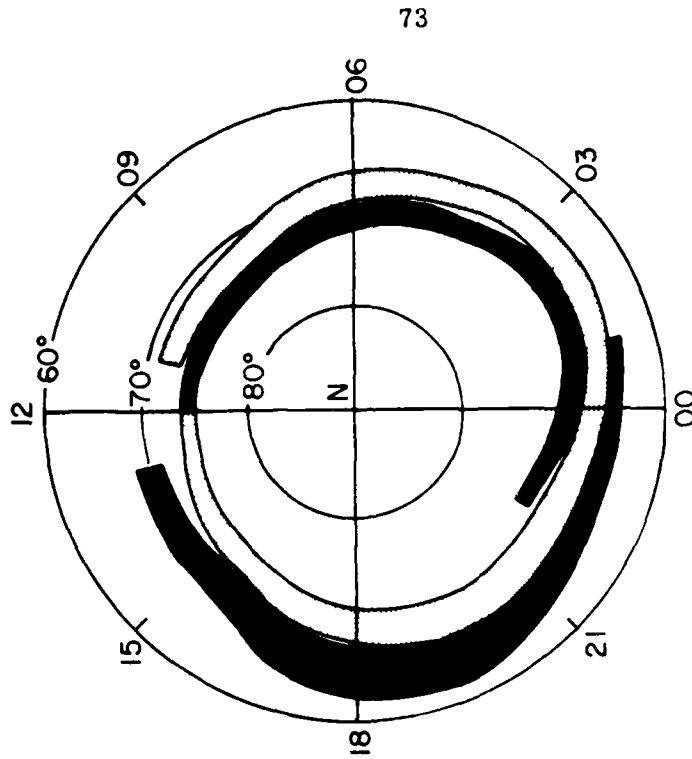
THEORY
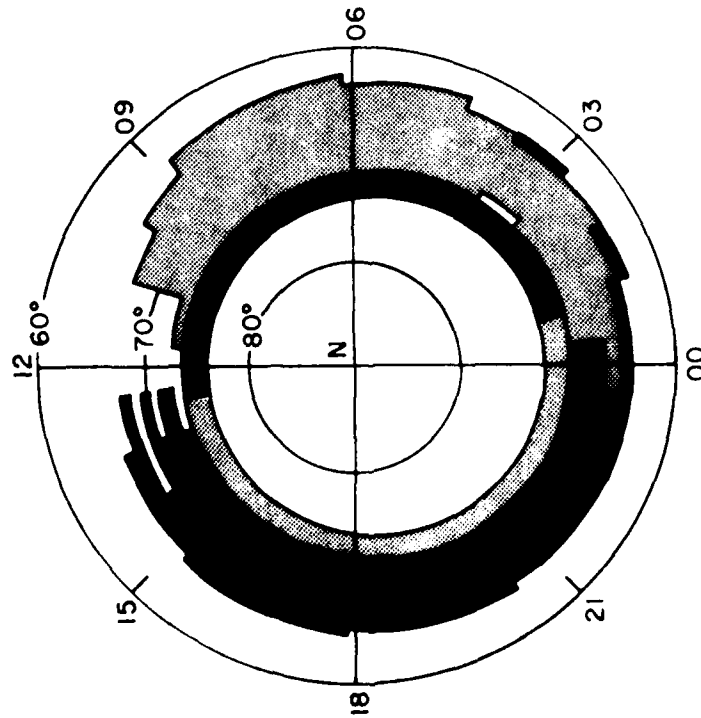
Current into ionosphere

Current away from ionosphere

Figure 14

CASE 1 IONOSPHERIC HALL CURRENT DENSITY

TIME = 10:50

IC=12

900.0 MAMP/M
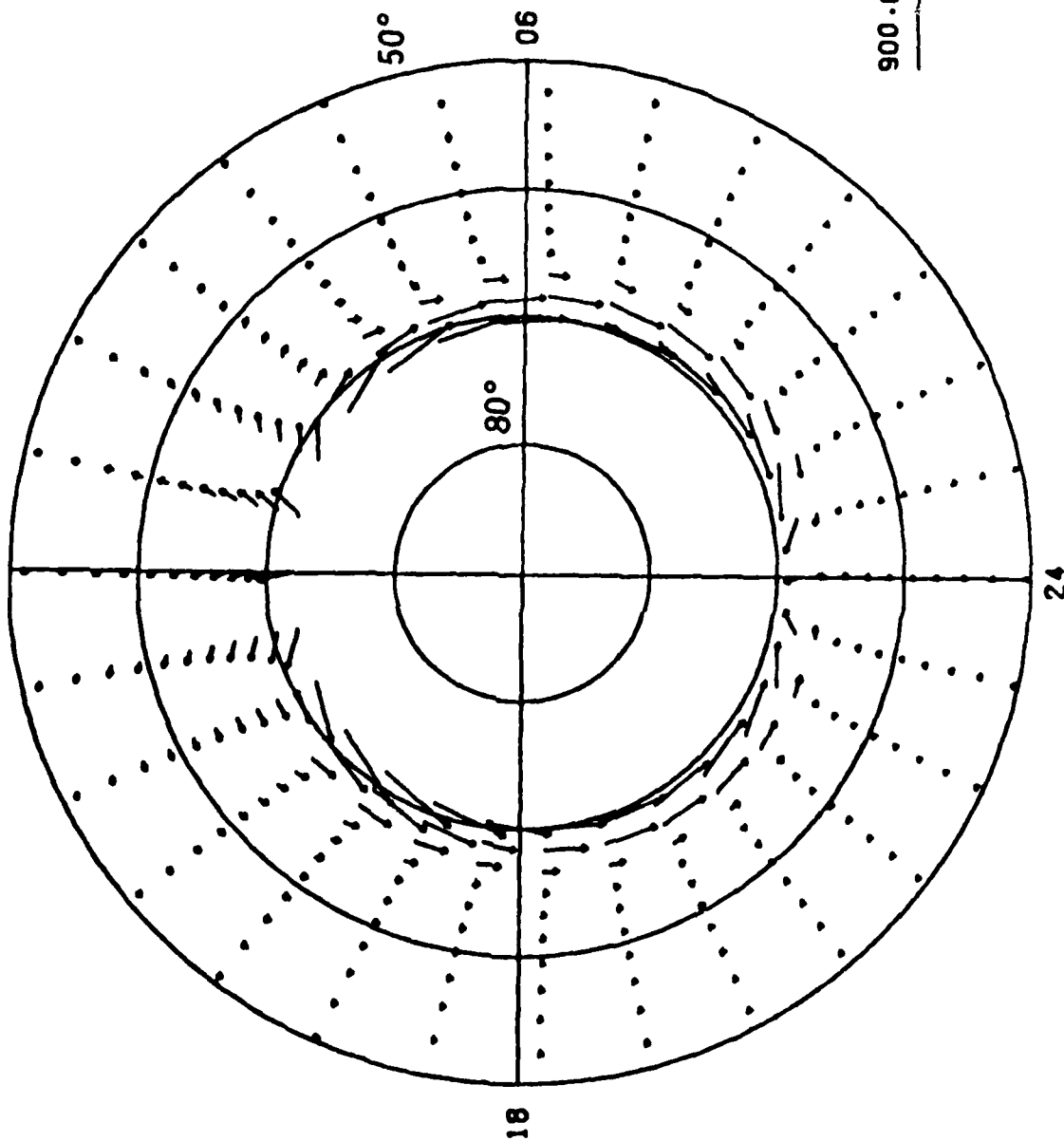
Figure 15

CASE 1 IONOSPHERIC PEDERSEN CURRENT DENSITY   IC=12

TIME = 10:50

800.0MAMP/M

Figure 16

76
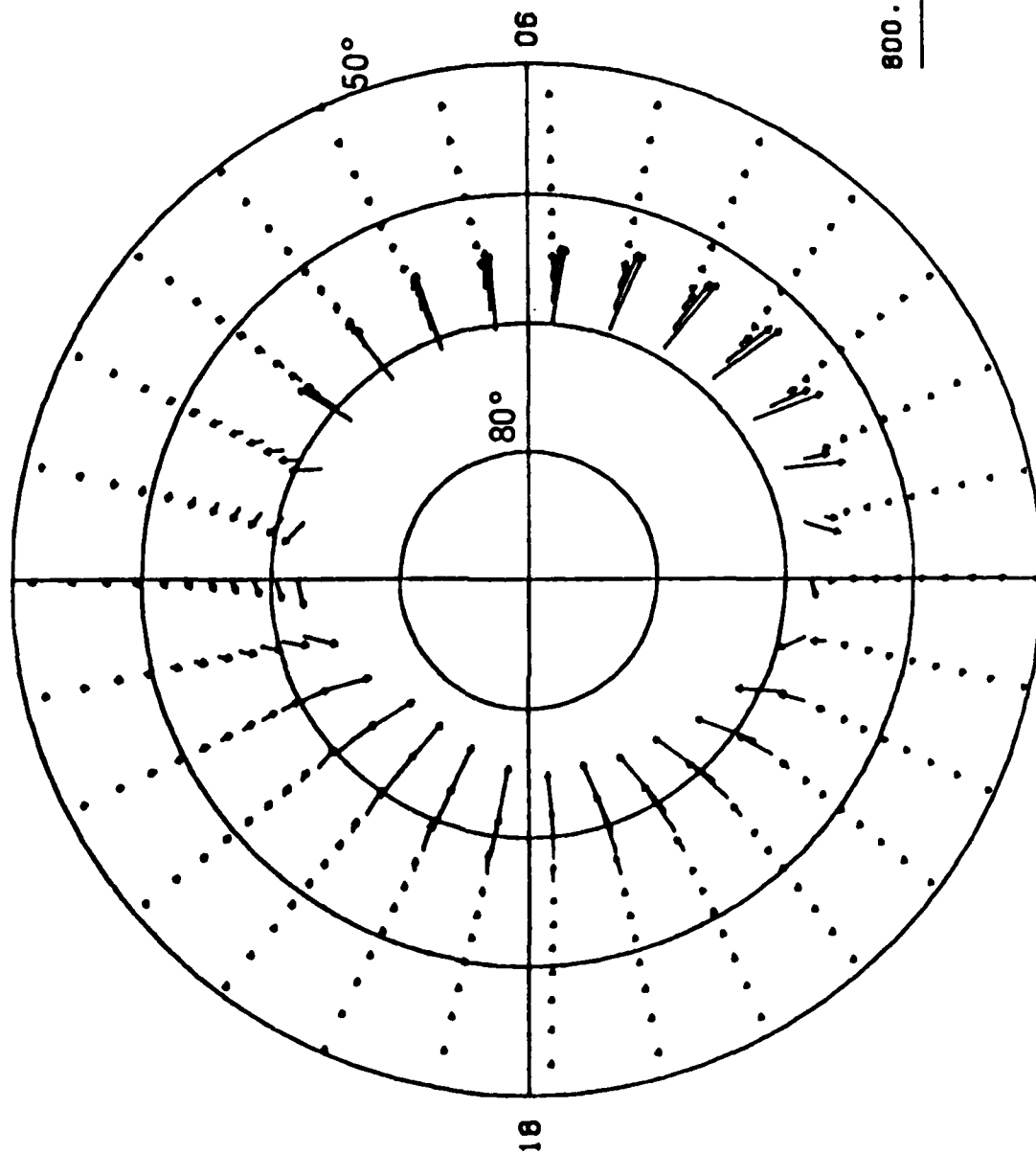
CASE 1   IONOSPHERIC TOTAL CURRENT DENSITY   IC=12

TIME = 10:50

Figure 17

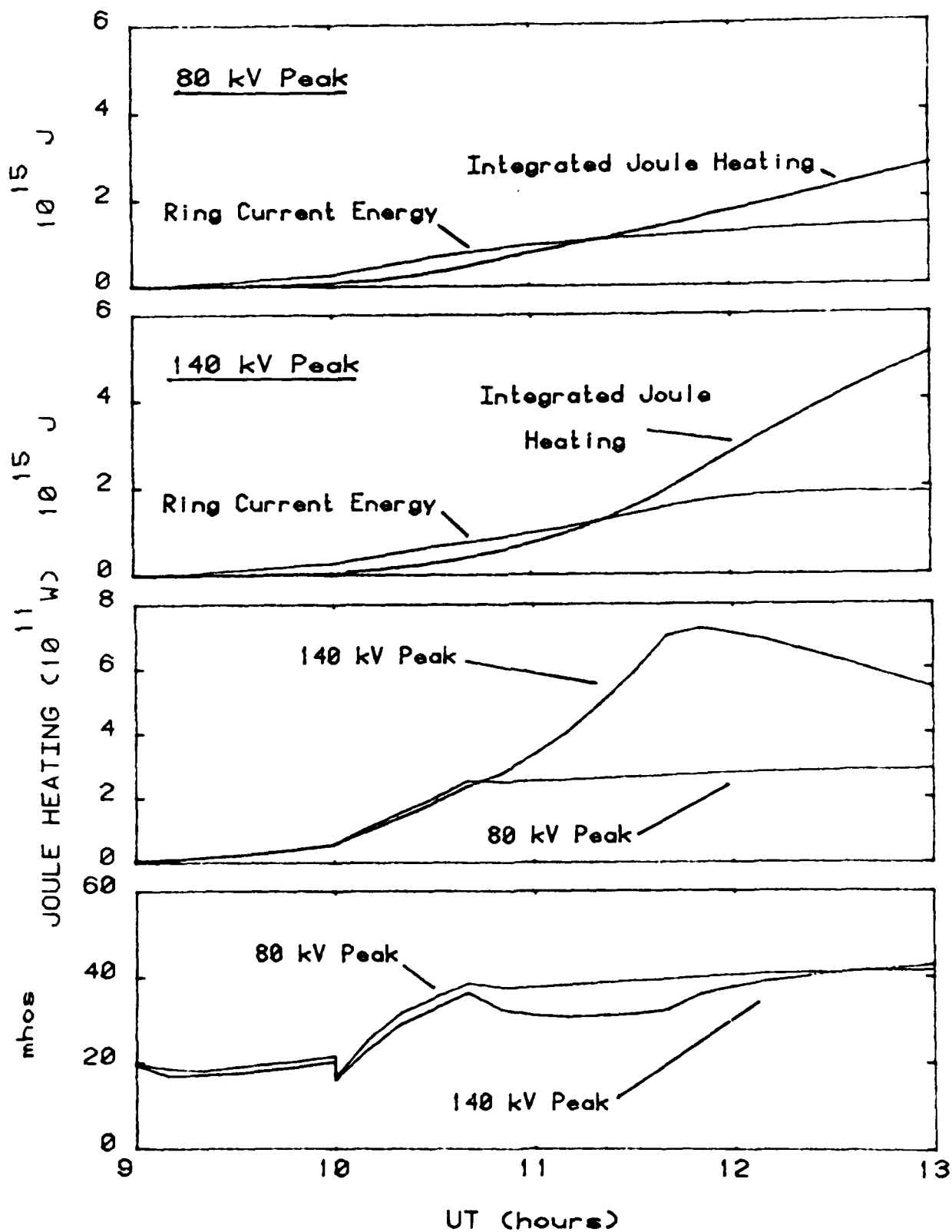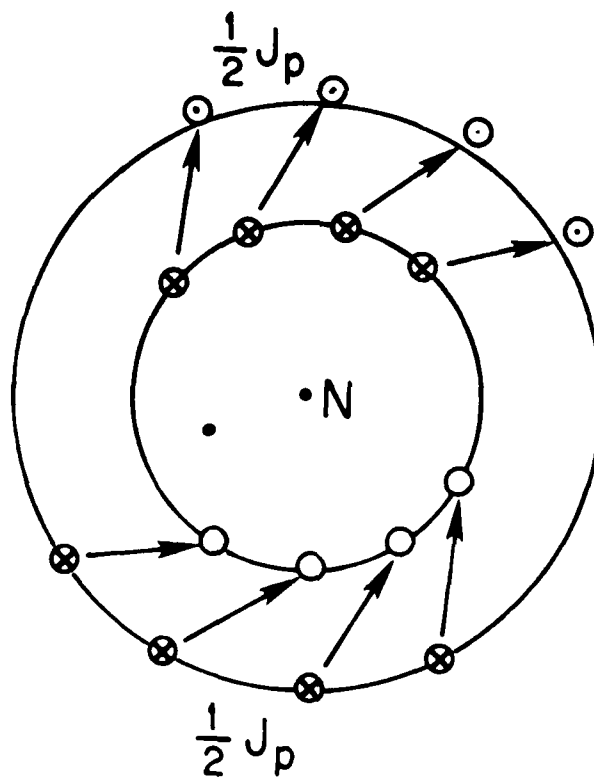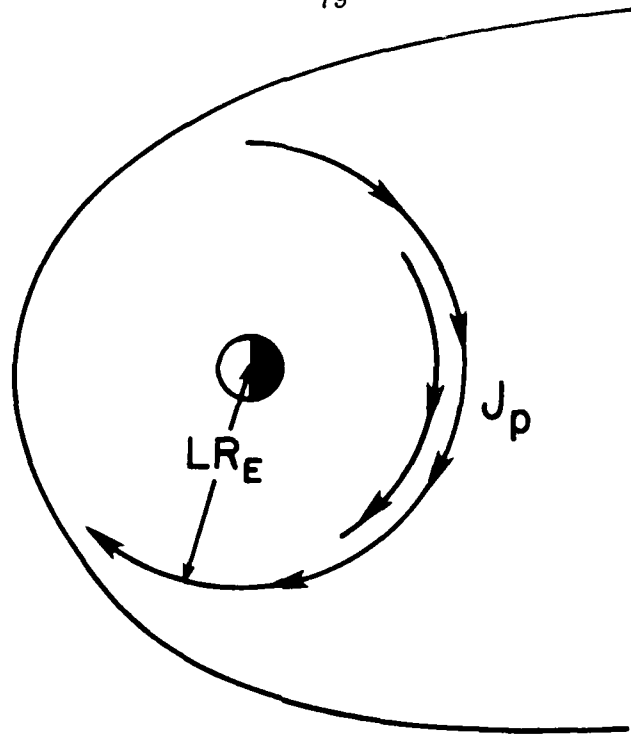Figure 18

Figure 19

J_p

LR_E

$\frac{1}{2} J_p$

$\cdot N$

$\frac{1}{2} J_p$

Figure 20

DATE
ILMED
8